

Synergistic impact of simultaneously assimilating radar- and radiometer-based soil moisture retrievals on the performance of numerical weather prediction systems

Yonghwan Kwon^{a*}, Sanghee Jun^a, Hyunglok Kim^b, Kyung-Hee Seol^a, In-Hyuk Kwon^a,
Eunkyu Kim^a, Sujeong Cho^a

^aKorea Institute of Atmospheric Prediction System, Seoul 07071, South Korea

^bDepartment of Environment and Energy Engineering, Gwangju Institute of Science and
Technology (GIST), Gwangju 61005, South Korea

*To whom correspondence may be addressed (yhwon@kiaps.org).

Revised manuscript submitted to *Hydrology and Earth System Sciences*

1 **Abstract**

2 The combined use of independent soil moisture data from radar and radiometer
3 measurements in data assimilation (DA) systems is expected to yield synergistic performance
4 gains due to their complementary strengths. This study evaluates the impact of
5 simultaneously assimilating soil moisture retrievals from ASCAT (Advanced SCATterometer)
6 and SMAP (Soil Moisture Active Passive) into the Korean Integrated Model (KIM) using a
7 weakly coupled DA framework based on the National Aeronautics and Space
8 Administration's Land Information System (LIS). The Noah land surface model (LSM)
9 within LIS, which is the same as that used in KIM, is used to simulate land surface states and
10 assimilate soil moisture retrievals. The impact of soil moisture DA is evaluated using
11 independent reference datasets, assessing its influence on soil moisture analysis and
12 numerical weather prediction performance. Overall, assimilating single-sensor soil moisture
13 data, ASCAT or SMAP, into the LSM improves global soil moisture analysis accuracy by 4.0%
14 and 10.5%, respectively, compared to the control case without soil moisture DA, achieving
15 the most significant enhancements in croplands. Relative to single-sensor soil moisture DA,
16 multi-sensor soil moisture DA yields more balanced skill enhancements for both specific
17 humidity and air temperature analyses and forecasts. The most pronounced synergistic
18 improvements by simultaneously assimilating both soil moisture products are observed in the
19 2-m air temperature analysis and forecast, especially when both soil moisture products have a
20 positive impact. Precipitation forecast skill also improves with multi-sensor soil moisture DA,
21 although the improvements are not consistent across regions and events. This paper discusses

22 remaining issues for future studies to further improve the weather prediction performance of
23 the KIM-LIS multi-sensor soil moisture DA system.

24

25 **Key words:** soil moisture data assimilation, multi-sensor, Korean Integrated Model, Land
26 Information System, numerical weather prediction, land-atmosphere coupled system

27

28 **1. Introduction**

29 Soil moisture is one of the decisive land surface state variables that control land-
30 atmosphere interactions associated with water and energy cycles (Gentine et al., 2011; Koster
31 et al., 2004; Tuttle and Salvucci, 2016) and that determine surface water infiltration,
32 percolation, and runoff (Assouline, 2013; Orth and Seneviratne, 2013). Many studies
33 underline the importance of accurate knowledge of the spatial and temporal soil moisture
34 variability for various hydrometeorological applications (e.g., Jalilvand et al., 2019; Shin and
35 Jung, 2014; Wanders et al., 2014; Yuan et al., 2011). Because of the long memory effect of
36 soil moisture, proper soil moisture initialization is a prominent part of numerical weather
37 prediction (NWP), particularly in the lower atmosphere (Dirmeyer and Halder, 2016; Drusch
38 and Viterbo, 2007; Jun et al., 2021; Koster et al., 2010; Kwon et al., 2024; van den Hurk et al.,
39 2012).

40 As a viable method to produce spatially and temporally complete, observation-constrained
41 estimates of soil moisture profiles (Bolten et al., 2010; Reichle et al., 2002a), assimilating
42 satellite-based soil moisture data into land surface models (LSMs) has been widely explored.
43 Soil moisture data assimilation (DA) optimally merges remotely-sensed near-surface soil

44 moisture observations with modeled soil moisture estimates based on their respective
45 uncertainties (Kumar et al., 2008a; Reichle et al., 2008), and it can generate soil moisture
46 estimates superior to either observations or models alone when the relative size of the
47 uncertainties is properly characterized (Liu et al., 2011; Blyverket et al., 2019). A number of
48 studies have applied soil moisture DA to improve flood and drought forecasts (e.g., Azimi et
49 al., 2020; Gavahi et al., 2022; Laiolo et al., 2016), streamflow and runoff predictions (e.g.,
50 Baugh et al., 2020; Brocca et al., 2010; Lievens et al., 2016), irrigation characterization (e.g.,
51 Kwon et al., 2022; Nair and Indu, 2019), and evaporative flux estimates (e.g., Li et al., 2020;
52 Pipunic et al., 2013). In particular, it has been demonstrated that the assimilation of satellite-
53 based soil moisture retrievals into LSMs that are coupled to atmospheric models has a
54 positive impact on weather forecast skill (e.g., Draper and Reichle, 2019; Jun et al., 2021;
55 Kwon et al., 2024; Lin and Pu, 2020; Lodh et al., 2022; Yin et al., 2019).

56 In addition to DA methods, a variety of alternative data fusion techniques have been
57 widely explored to integrate soil moisture information from different sources, including
58 remote sensing products, in-situ measurements, model simulations, and reanalysis datasets.
59 One group of approaches relies on statistical methods (e.g., Min et al., 2022; Wang et al.,
60 2021; Xie et al., 2022), such as unweighted averaging, linear weight fusion, and emergent
61 constraint. Another group leverages machine learning (e.g., Huang et al., 2023; Lamichhane
62 et al., 2025; Long et al., 2019; Zhang et al., 2022, Zeng et al., 2024) and deep learning
63 techniques (e.g., Fuentes et al., 2022; Huang et al., 2022; Jiang et al., 2025; Singh and Gaurav,
64 2023; van der Schalie et al., 2018). These machine learning and deep learning approaches are
65 rapidly gaining prominence because of their ability to incorporate diverse data sources and to

66 capture complex, nonlinear relationships between datasets (Huang et al, 2022; Zeng et al.,
67 2024). While different fusion approaches have distinct strengths and limitations, this study is
68 devoted to DA methods, with the goal of improving model-based soil moisture estimates that
69 interact with atmospheric processes in operational land-atmosphere coupled systems, thereby
70 enhancing weather forecasts.

71 Microwave satellite systems provide useful information to retrieve surface soil moisture
72 data at the global scale owing to their sensitivity to soil dielectric properties that mainly
73 depend on soil water content and surface roughness (Schmugge et al., 1986). Many satellite
74 soil moisture products have been generated from microwave observations at different
75 frequencies (i.e., X, C and L-band) using various retrieval algorithms in different systems
76 during the past several decades (Kumar et al., 2019; Nair and Indu, 2018). Among them, the
77 Advanced SCATterometer (ASCAT) (e.g., Bartalis et al., 2007; Wagner et al., 2013), Soil
78 Moisture Active Passive (SMAP) (e.g., Chan et al., 2018; O'Neill et al., 2021), and Soil
79 Moisture and Ocean Salinity (SMOS) (e.g., Kerr et al., 2012) are relatively modern sensors
80 that have been widely used in soil moisture DA studies (e.g., Blyverket et al., 2019; Jun et al.,
81 2021; Khaki and Awange, 2019; Kolassa et al., 2017; Kumar et al., 2019; Kwon et al., 2022,
82 2024; Nair and Indu, 2019; Renzullo et al., 2014; Seo et al., 2021; Tangdamrongsub et al.,
83 2020). In addition, most recently, Nguyen et al. (2025) have demonstrated the usefulness of
84 soil moisture retrievals based on signals from the Global Navigation Satellite Systems.
85 Kumar et al. (2019) report that soil moisture retrievals from these modern sensors exhibit
86 better performance in DA systems than those from older sensors.

87 The present study focuses on the use of the ASCAT and SMAP soil moisture products to
88 improve modeled soil moisture estimates via assimilation. The ASCAT soil moisture product
89 is generated from active microwave backscatter measurements at C-band (5.3 GHz) while the
90 SMAP soil moisture data is based on passive microwave satellite systems, which utilize
91 naturally emitted brightness temperature from the Earth's surface at an L-band (1.4 GHz)
92 frequency. The C-band (i.e., ASCAT) and L-band (i.e., SMAP) sensors typically provide soil
93 moisture information for soil depth of 0–2 cm and 0–5 cm, respectively (Kim et al., 2018).
94 Compared to passive radiometers, radar observations (i.e., ASCAT) have smaller footprint
95 sizes (i.e., finer spatial resolutions) and thus provide better spatial details of soil moisture
96 (Nair and Indu, 2019). However, ASCAT has large uncertainties over regions of complex
97 topography due to multiple scattering effects (Dobson and Ulaby, 1986). In contrast,
98 radiometer (SMAP) observations are more sensitive to the presence of soil moisture than
99 active radars (Kolassa et al., 2017), but the accuracy of their soil moisture products is
100 strongly influenced by vegetation water content and surface temperature (Paloscia and
101 Pampaloni, 1988).

102 Because of their complementary advantages, better soil moisture estimates can be obtained
103 by assimilating the soil moisture data from multiple sources into the model-simulated soil
104 moisture within a DA system. There have been some efforts to synergistically combine
105 multiple active and passive observations for spatially and temporally improved soil moisture
106 retrievals such as the European Space Agency Climate Change Initiative (ESA CCI; Dorigo
107 et al., 2017). In addition, one of the key goals of the SMAP mission was to utilize both active
108 and passive sensors on the same satellite platform to retrieve high spatial resolution global

109 near-surface soil moisture data with great accuracy (Entekhabi et al., 2010). However, due to
110 mechanical malfunction of the SMAP radar, alternative radar observations from other
111 satellites (e.g., Sentinel-1) have been combined with the SMAP radiometer data to maintain
112 data continuity (Das et al., 2019). Meanwhile, Kolassa et al. (2017) and Nair and Indu (2019)
113 demonstrate that simultaneously assimilating individual radar- and radiometer-based soil
114 moisture retrievals achieves comparable overall performance to the assimilation of the
115 blended (i.e., radar + radiometer) soil moisture products. In this study, we do not aim to
116 retrieve or assimilate blended soil moisture products from multiple satellite measurements.
117 Instead, we independently utilize soil moisture data from each sensor (i.e., ASCAT and
118 SMAP) within a land-atmosphere coupled DA system, while also incorporating both
119 observations separately rather than combining them spatially. This approach may provide a
120 more effective way to account for the relative reliability of each sensor in soil moisture
121 assimilation (Kolassa et al., 2017), and offers greater flexibility for assimilating various soil
122 moisture products simultaneously in different combinations.

123 This study is built on a land-atmosphere coupled DA system, which consists of the
124 Korean Integrated Model (KIM; Hong et al., 2018) and the National Aeronautics and Space
125 Administration (NASA) Land Information System (LIS; Kumar et al., 2006, 2008b; Peters-
126 Lidard et al., 2007). Hereafter, this system is referred to as the KIM-LIS coupled system. As
127 an operational global NWP model at the Korea Meteorological Administration, KIM has
128 been developed by the Korea Institute of Atmospheric Prediction Systems (KIAPS). KIM has
129 capabilities of conducting short-to-medium-range and extended-range weather forecasts, and
130 of implementing atmospheric DA to generate improved atmospheric initial conditions for the

131 forecasts (Kwon et al., 2018). Land DA in the current Korea Meteorological Administration's
132 operational NWP system is based on the KIM-LIS coupled system and ingests the ASCAT
133 soil moisture retrievals to constrain the modeled soil moisture (Jun et al., 2021). Recently
134 Kwon et al. (2024) have demonstrated the feasibility of assimilating the SMAP soil moisture
135 retrievals into the Noah LSM (Ek et al., 2003) within the KIM-LIS system to enhance the
136 global soil moisture estimates and weather forecast performance of KIM.

137 While several studies have explored the simultaneous use of radar and radiometer-based
138 soil moisture data in offline land DA systems, mainly to improve soil moisture estimates and
139 associated hydrological processes (e.g., Draper et al., 2012; Khaki and Awange, 2019; Khaki
140 et al., 2019, 2020; Kolassa et al., 2017; Kumar et al., 2019; Nair and Indu, 2019; Renzullo et
141 al., 2014; Seo et al., 2021; Tangdamrongsub et al., 2020), only a few have investigated their
142 impacts on atmospheric forecasts in land-atmosphere coupled NWP systems (e.g., de Rosnay
143 et al., 2022; Draper and Reichle, 2019; Fairbairn et al., 2024). Even among studies using
144 coupled forecast systems, most assimilate only ASCAT and SMOS together, despite evidence
145 that SMAP provides high-quality soil moisture data (e.g., Bhuiyan et al., 2018; Chan et al.,
146 2018; Colliander et al., 2017) and often outperforms other sensors (Kumar et al., 2018). In
147 this regard, the novelty of this study is the combined use of ASCAT and SMAP soil moisture
148 products in the KIM-LIS-based land-atmosphere coupled DA system, demonstrating their
149 feasibility.

150 The present study aims to evaluate the relative (individual) and combined performance of
151 C-band radar-based (i.e., ASCAT) and L-band radiometer-based (i.e., SMAP) surface soil
152 moisture products in improving the global soil moisture analysis and atmospheric

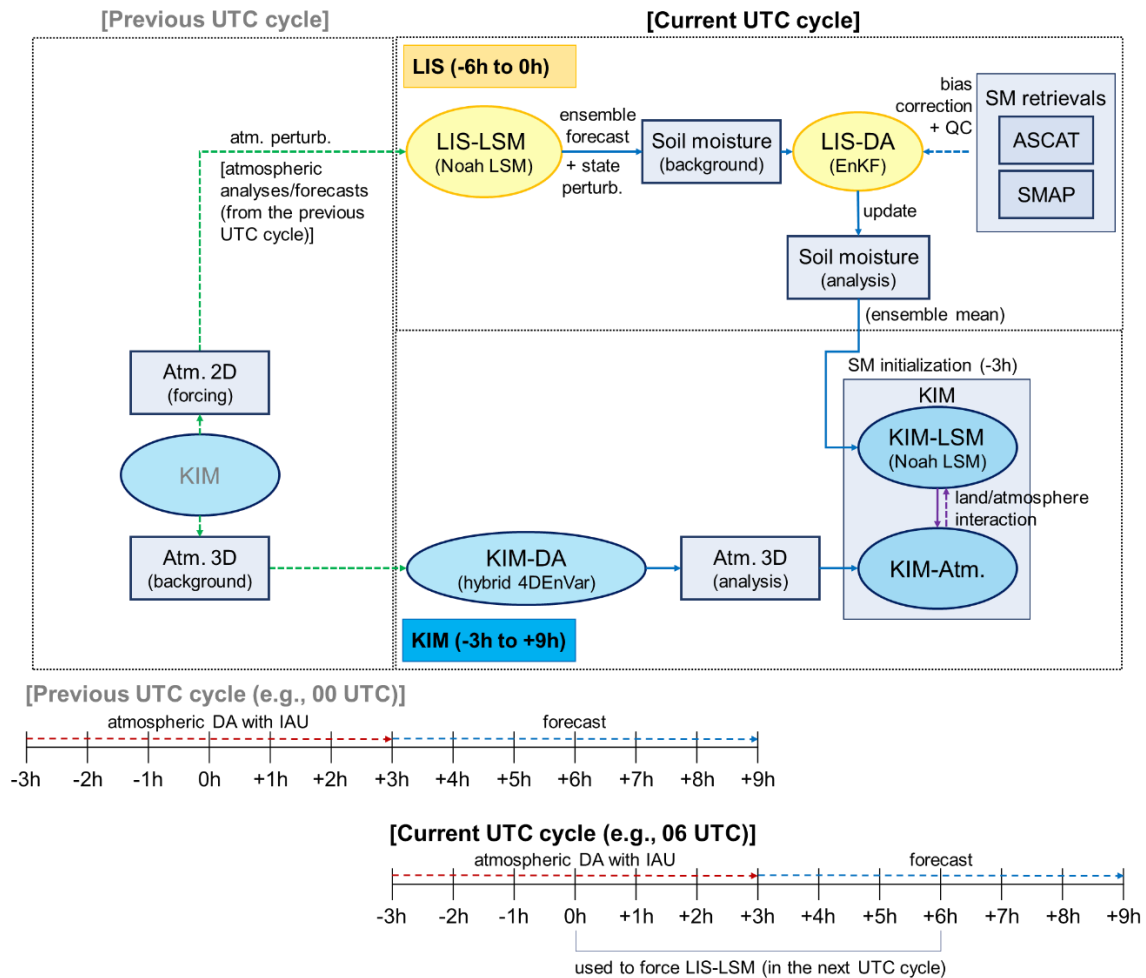
153 analysis/forecast via assimilation within the KIM-LIS coupled system. We first assimilate
154 each soil moisture product individually into the Noah LSM in the KIM-LIS system over the
155 global domain, and compare their respective performance gains. The synergistic impacts of
156 simultaneously assimilating the ASCAT and SMAP soil moisture retrievals on the global
157 estimates of lower atmospheric variables are then investigated.

158

159 **2. KIM-LIS-based weakly coupled DA system**

160 The KIM-LIS system (Jun et al., 2021; Kwon et al., 2024) is a weakly coupled DA
161 system, in which the land analysis and atmospheric analysis are implemented independently
162 (Figure 1). The present study uses the KIM version 3.9 and LIS version 7.4, the same
163 versions as those used in Kwon et al. (2024). KIM (Hong et al., 2018) is composed of a
164 global non-hydrostatic dynamical core using a cubed-sphere grid system with up to 91
165 vertical levels on a hybrid-sigma coordinate system (Song et al., 2017; Kwon et al., 2018).
166 LIS (Kumar et al., 2006, 2008b; Peters-Lidard et al., 2007) is a land surface hydrological
167 modeling and DA system where various LSMs, DA schemes, and surface coordinate systems
168 are available for different applications. In this study, the latitude-longitude grid system is
169 used for LIS.

170



171
 172 **Figure 1.** Schematic diagram of the KIM-LIS-based land-atmosphere weakly coupled data
 173 assimilation (DA) system. The figure outlines the process flow between KIM and LIS in one
 174 UTC cycle that is performed four times (i.e., 00, 06, 12, and 18 UTC cycles) a day. (IAU:
 175 incremental analysis update, QC: quality control)
 176

177 KIM and LIS employ separate versions of the Noah LSM, referred to as KIM-LSM and
 178 LIS-LSM, respectively, in Figure 1 to simulate land-surface hydrological processes. In the
 179 Noah LSM (Ek et al., 2003), a soil column (2-m total depth) is discretized into four layers
 180 with the standard thickness of 0.1 m, 0.3 m, 0.6 m, and 1.0 m from surface to bottom for
 181 estimation of soil moisture and soil temperature. The original Noah version of KIM-LIS is

182 2.7.1, but it has undergone many updates based on later versions of the Noah LSM with
183 additional modifications to physical parameterizations and land surface inputs to achieve
184 optimal performance of KIM (Koo et al., 2017). As in Jun et al. (2021) and Kwon et al.
185 (2024), the Noah LSM version 3.3 implemented within LIS is used for LIS-LSM by applying
186 the same modifications to ensure consistency between KIM-LSM and LIS-LSM.

187 The KIM-LIS coupled system conducts a forecast/analysis cycle every 6 hours [i.e., 00,
188 06, 12, and 18 Coordinated Universal Time (UTC) cycles] where KIM and LIS run for time
189 windows of 12 hours (i.e., -3 h to +9 h) and 6 hours (i.e., -6 h to 0 h), respectively, as
190 outlined in Figure 1. LIS-LSM (i.e., Noah LSM) creates an ensemble of background (prior)
191 soil moisture estimates forced by atmospheric fields from the previous UTC cycle (0 h to +6
192 h) KIM analysis/forecast, which are remapped from the cubed-sphere grid to the latitude-
193 longitude grid and perturbed by adding Gaussian random perturbations. Additional random
194 perturbations are imposed on the prior soil moisture estimates, which are then merged with
195 remotely-sensed soil moisture retrievals using the ensemble Kalman filter (EnKF) method
196 (Evensen, 1994; Reichle et al., 2002b) to generate the soil moisture analysis. This sequential
197 EnKF procedure (i.e., soil moisture forecast and analysis) is performed from -6 h to 0 h in
198 the current UTC cycle. LIS writes land outputs every 3 hours (i.e., at -3 h and 0 h) and
199 generates a restart file at 0 h. The restart file contains the complete set of model state
200 variables at that time, enabling LIS-LSM to be consistently re-initialized in the subsequent
201 UTC cycle. The soil moisture analysis from LIS at -3 h is remapped from the latitude-
202 longitude grid to the cubed-sphere grid, and is used to initialize the soil moisture conditions
203 of KIM-LSM that provides land boundary conditions for the KIM forecast and analysis from

204 -3 h to +9 h in the current UTC cycle. The atmospheric analysis is performed based on the
205 hybrid four-dimensional ensemble variational (hybrid 4DEnVar) DA method (Song et al.,
206 2017; Kwon et al., 2018). To minimize the initialization shock resulting from the atmospheric
207 DA, the four-dimensional incremental analysis update (4DIAU; Lorenc et al.,2015) is
208 employed within an atmospheric assimilation window (i.e., -3 h to + 3h). KIM is further run
209 without DA until +9 h, and the KIM analysis/forecasts from 0 h to +6 h in the current UTC
210 cycle are then used for the next UTC cycle LIS implementation.

211 Although the remapping procedures required to share information between KIM and LIS
212 may introduce some error, Jun et al. (2021) and Kwon et al. (2024) have demonstrated that
213 soil moisture DA based on the KIM-LIS system provides beneficial impacts on improving the
214 weather forecast performance of KIM. In addition, the KIM-LIS coupled system, which
215 employs the LIS-based land DA, has several advantages: (1) it can readily leverage the
216 existing land DA functions of LIS, and (2) it allows straightforward implementation of new
217 land DA developments due to LIS's extensible framework.

218

219 **3. Satellite-based soil moisture retrievals**

220 We assimilate the satellite-based near-surface soil moisture retrievals from ASCAT and
221 SMAP individually and together into the Noah LSM to constrain the modeled soil moisture
222 estimates. A brief explanation of the soil moisture products is given below.

223

224

225

226 **3.1. Active soil moisture product: ASCAT**

227 ASCAT is a real aperture radar onboard the Meteorological Operational (MetOp)
228 satellites (i.e., MetOp-A, MetOp-B, and MetOp-C), and measures radar backscatter at C-band
229 (5.3 GHz) VV (vertical transmit vertical receive) polarization (Wagner et al., 2013). The
230 equator crossing times of the MetOp satellites are 9:30 am/pm local solar time (LST) for the
231 descending and ascending overpasses, respectively, with a revisit frequency of 1–3 days. The
232 ASCAT soil moisture is retrieved based on the Vienna University of Technology (TU Wien)
233 change detection algorithm (Wagner et al., 1999, 2010), and provides an estimate of the
234 degree of water saturation (ranging between 0 and 100%) of the top 0–2 cm soil layer.

235 We use the MetOp-B/C ASCAT near-real time soil moisture product at 12.5 km swath
236 grid. The soil moisture product used in this study was obtained directly from the European
237 Organisation for the Exploitation of Meteorological Satellites (EUMETSAT) for use in the
238 Korea Meteorological Administration’s operational weather prediction system while the same
239 product can be downloaded from the EUMETSAT Earth Observation Portal
240 (<https://eoportal.eumetsat.int>).

241

242 **3.2. Passive soil moisture product: SMAP**

243 The SMAP mission provides volumetric soil moisture ($\text{m}^3 \text{m}^{-3}$) for the top 0–5 cm of the
244 soil, derived from L-band (1.4 GHz) passive microwave radiometer measurements
245 (Entekhabi et al., 2010). It has a revisit cycle of 2–3 days, with local equator-crossing times
246 of 6 am (descending) and 6 pm (ascending).

247 The present study uses the SMAP Level 2 (L2) Radiometer Half-Orbit 36 km Equal Area
248 Scalable Earth (EASE)–Grid soil moisture data (SPL2SMP version 9, O’Neill et al., 2021),
249 which is obtained from the National Snow and Ice Data Center (NSIDC,
250 <https://n5eil01u.ecs.nsidc.org/SMAP/SPL2SMP.009/>). The SMAP soil moisture retrievals
251 based on the Dual Channel Algorithm (DCA, Chaubell et al., 2020) are assimilated.

252

253 **3.3. Bias correction of the soil moisture data**

254 Typical DA algorithms are designed to correct random errors under the assumption of
255 unbiased state estimates between models and observations (Dee and da Silva, 1998).
256 However, there are generally large systematic discrepancies between modeled and satellite-
257 retrieved soil moisture because of their different representations of soil moisture associated
258 with the geophysical definition and horizontal/vertical scales (Koster et al., 2009; Kumar et
259 al., 2019). Therefore, soil moisture DA systems essentially employ appropriate bias
260 correction strategies to remove these systematic biases prior to assimilation, and thus to
261 comply with the DA assumption of unbiased models and observations (Kolassa et al., 2017;
262 Reichle and Koster, 2004). In this study, bias correction is implemented differently for the
263 ASCAT and SMAP soil moisture products. That is, we apply cumulative distribution function
264 (CDF) matching (Reichle and Koster 2004) and anomaly correction methods (Kwon et al.,
265 2022) to assimilate the ASCAT and SMAP soil moisture retrievals, respectively, into the
266 Noah LSM within the KIM-LIS coupled system. The use of the anomaly correction method
267 for SMAP follows our previous investigations (Kwon et al., 2022, 2024) aiming to minimize
268 the loss of useful information from the original data through bias correction. In contrast,

269 traditional CDF matching is applied to ASCAT, since the anomaly correction method is not
270 applicable due to difference in soil moisture data type between ASCAT (soil wetness index)
271 and the model (volumetric soil moisture in $\text{m}^3 \text{m}^{-3}$). Further details are provided in the
272 following two paragraphs.

273 The CDF matching is a commonly used bias correction method in soil moisture DA.
274 Through the CDF matching, in this study, the ASCAT soil wetness index data are
275 transformed to volumetric soil moisture ($\text{m}^3 \text{m}^{-3}$) by correcting all the statistical moments of
276 the original ASCAT data to those of the Noah-simulated soil moisture. Existing soil moisture
277 DA studies use two different CDF matching approaches. One uses a lumped CDF computed
278 using all seasons data (i.e., pixel-wise single CDF for each data type) (e.g., Draper et al.,
279 2011, 2012; Kumar et al., 2009, 2014; Reichle et al., 2007) while the other uses monthly-
280 stratified CDFs (i.e., pixel-wise 12 CDFs for each data type) (e.g., Jun et al., 2021; Kumar et
281 al., 2015; Kwon et al., 2022, 2024; Santanello Jr et al., 2016). Kumar et al. (2015) and
282 Santanello Jr et al., (2016) suggest using the monthly CDF rather than the lumped CDF to
283 mitigate spurious statistical artifacts in the bias-corrected soil moisture by the CDF matching.
284 Kwon et al. (2024) show that abnormal fluctuations are witnessed in the lumped CDF-based
285 rescaled soil moisture, particularly in dry periods, and Kwon et al. (2022) demonstrate that
286 soil moisture DA employing the monthly CDF achieves better soil moisture analysis than that
287 applying the lumped CDF matching. Based on these previous findings, we implement the
288 monthly CDF matching for the ASCAT soil moisture DA.

289 The anomaly correction method, proposed by Kwon et al. (2022), is a simpler alternative
290 to traditional bias correction approaches. It aims to reduce the reliance of DA systems on

291 rescaling methods like the CDF matching, which is known to cause significant information
292 loss in the original soil moisture data, especially when human-induced processes (e.g.,
293 irrigation activities), poorly represented in models, are the dominant source of systematic
294 discrepancies between observations and models (Kumar et al., 2015; Nearing et al., 2018).
295 Instead of rescaling the SMAP soil moisture retrievals, the anomaly correction approach
296 obtains the soil moisture temporal variability (i.e., anomaly) information by subtracting the
297 long-term soil moisture mean from the original SMAP data. The extracted SMAP soil
298 moisture anomaly is added to the long-term mean of the modeled soil moisture, which is then
299 assimilated into the LSM. The anomaly correction assumes that the systematic bias between
300 observations and models is dominated by the climatological mean difference and higher
301 moment (e.g., standard deviation) differences are negligible. Kwon et al. (2022) and Kwon et
302 al. (2024) demonstrate that the SMAP soil moisture data and Noah-simulated soil moisture
303 satisfy this underlying assumption over the continental United States and global domain,
304 respectively. In particular, Kwon et al. (2024) show that the anomaly correction-based SMAP
305 soil moisture DA is effective in improving the global soil moisture estimates and weather
306 forecast skill of the KIM-LIS coupled system that employs the Noah LSM.

307

308 **3.4. Quality control of the soil moisture data**

309 The ASCAT and SMAP soil moisture retrievals undergo quality control before DA by
310 removing inaccurate or uncertain soil moisture observations based on strategies employed in
311 previous soil moisture DA studies (e.g., Blyverket et al., 2019; Draper et al., 2012; Ferguson
312 et al., 2020; Jun et al., 2021; Kolassa et al., 2017; Kumar et al., 2014, 2019; Kwon et al., 2022,

313 2024; Nair and Indu, 2019). Firstly, before bias correction, the soil moisture data are
314 discarded when the data quality flags provided with each soil moisture product indicate that
315 the data accuracy is impacted by open water bodies, dense vegetation, urban areas,
316 precipitation, snow cover, frozen ground, complex topography, or anthropogenic Radio
317 Frequency Interference (RFI). Especially, the ASCAT soil moisture retrievals are assimilated
318 only when the Estimated Soil Moisture Error (ESME) is less than 16%, and the topographic
319 complexity and wetland fraction are below 20% and 15%, respectively, as applied in Jun et al.
320 (2021). These uncertainty thresholds are slightly higher than those used in Draper et al. (2012)
321 and Kolassa et al. (2017) for the purpose of utilizing more data in a near-real time operational
322 DA system.

323 Secondly, the model-based quality control is additionally applied to both ASCAT and
324 SMAP after bias correction. Specifically, assimilation of ASCAT and SMAP soil moisture
325 into the Noah LSM is not performed in the case that (1) model background estimates indicate
326 active precipitation events or frozen/snow-covered soil conditions, that (2) the model land
327 cover type and green vegetation fraction inputs from the Moderate resolution imaging
328 spectroradiometer (MODIS) International Geosphere-Biosphere Programme (IGBP) data
329 (Friedl et al., 2002) and the National Centers for Environmental Prediction (NCEP),
330 respectively, indicate that a grid cell is classified as forests or has green vegetation fraction
331 greater than 0.7, or that (3) bias-corrected soil moisture retrievals are close to wilting point or
332 saturation.

333

334

335 **4. DA methods**

336 **4.1. Atmospheric DA**

337 Atmospheric DA in KIM is based on a hybrid four-dimensional ensemble variational
338 (hybrid 4DEnVar) DA method as described in Kwon et al. (2018) and Song et al. (2017). In
339 this study, we assimilate both conventional and non-conventional atmospheric data including
340 the Advanced Microwave Sounding Unit-A (AMSU-A), Atmospheric Motion Vectors
341 (AMVs), Microwave Humidity Sounder (MHS), Global Positioning System Radio
342 Occultation (GPS-RO), Infrared Atmosphere Sounding Interferometer (IASI), Advanced
343 Technology Microwave Sounder (ATMS), Cross-track Infrared Sounder (CrIS), and
344 observations obtained from surface, aircraft, and sonde. The KIM Package of Observation
345 Processing (KPOP, Kang et al., 2019) is employed to preprocess (e.g., quality control and
346 bias correction) the observations before assimilation. Details of the KIM hybrid 4DEnVar
347 DA scheme are provided in Text S1 and in Kwon et al. (2018) and Song et al. (2017).

348

349 **4.2. Land soil moisture DA**

350 In the KIM-LIS coupled system, land DA is conducted by the LIS-DA subsystem (Figure
351 1) in which various DA schemes are available. The current study applies a 1-dimensional
352 EnKF method (Reichle et al., 2002b) to assimilate satellite soil moisture retrievals (i.e.,
353 ASCAT and SMAP) into the Noah LSM. The EnKF is one of the widely used DA schemes
354 for nonlinear hydrological applications (e.g., Cho et al., 2023; Crow and Van den Berg, 2010;
355 Draper and Reichle, 2019; Kim et al., 2021a; Kwon et al., 2019, 2021; Reichle et al., 2023;

356 Renzullo et al., 2014; Xu et al., 2021) because of its relatively flexible and computationally
357 efficient nature (Keppenne, 2000).

358 Within the EnKF-based DA system, model forecasts and analysis updates are performed
359 alternately. That is, the ensemble forecasts of model prognostic state variables are propagated
360 forward in time until observations are available, and the forecasted states are updated in the
361 assimilation step when and where observations exist. The resulting analysis ensemble is then
362 used as the initial condition for the next model forecast. In this study, the control vectors that
363 are directly updated by assimilating the ASCAT and SMAP soil moisture retrievals include
364 the Noah LSM estimates of soil moisture at four soil layers while other related
365 hydrometeorological variables are adjusted through model physics in subsequent model
366 integrations. As we conduct the 1-dimensional EnKF, the soil moisture analysis in a given
367 grid is produced independently of neighboring grids.

368 The EnKF increments are determined depending on the relative uncertainties (error
369 variances) of model and observation. The model uncertainty (background error covariance) is
370 represented by the ensemble forecast spread (ensemble size of 20), which is obtained at each
371 grid by randomly perturbing the atmospheric variables from KIM including shortwave
372 radiation, longwave radiation, and precipitation, and by additionally (randomly) perturbing
373 the Noah LSM-simulated soil moisture estimates. Shortwave radiation and precipitation are
374 perturbed by applying log-normally distributed multiplicative perturbations with standard
375 deviations of 0.3 and 0.5, respectively, while normally distributed additive perturbations are
376 applied to longwave radiation (with a standard deviation of 50 W m^{-2}) and the soil moisture
377 (SM) estimates at four soil layers [with standard deviations of 0.01, 0.006, 0.003, and 0.0015

378 $\text{m}^3 \text{m}^{-3}$ for SM1 (top layer), SM2, SM3, and SM4 (bottom layer), respectively]. First-order
 379 autoregressive temporal correlations and cross-variable correlations are also considered
 380 during the perturbation (Table 1), whereas horizontal error correlations are neglected. The
 381 perturbation parameters used in this study are determined based on Kumar et al. (2017, 2019)
 382 and Reichle et al. (2008), and have also been effectively applied in Jun et al. (2021) and
 383 Kwon et al. (2024).

384 **Table 1.** Perturbation parameter values used for autoregressive temporal correlation and cross
 385 correlations between different variables (SW: shortwave radiation, LW: longwave radiation,
 386 P: precipitation, SM1: top layer soil moisture, SM2: second layer soil moisture, SM3: third
 387 layer soil moisture, and SM4: bottom layer soil moisture).

Perturbed variables	Time scale of first-order autoregressive temporal correlations (hour)	Cross correlations with perturbations in			
		SW	LW	P	
<u>KIM atmospheric forcing</u>					
SW	24	1.0	-0.5	-0.8	
LW	24	-0.5	1.0	0.5	
P	24	-0.8	0.5	1.0	
<u>Noah LSM soil moisture</u>					
SM1	12	1.0	0.6	0.4	0.2
SM2	12	0.6	1.0	0.6	0.4
SM3	12	0.4	0.6	1.0	0.6
SM4	12	0.2	0.4	0.6	1.0

388

389 The spatially and temporally constant observation error standard deviations of 10% and
 390 $0.02 \text{ m}^3 \text{m}^{-3}$ are applied for ASCAT and SMAP soil moisture retrievals, respectively, based
 391 on previous DA studies (e.g., Dorigo et al., 2010; Draper et al., 2012; Ferguson et al., 2020;
 392 Kolassa et al., 2017; Kwon et al. 2022, 2024). In the KIM-LIS coupled system, the ASCAT-
 393 derived soil wetness index data are scaled into the Noah LSM soil moisture climatology (in
 394 $\text{m}^3 \text{m}^{-3}$) through the CDF matching (see Section 3.3) to remove the systematic bias between
 395 the ASCAT soil moisture and Noah-simulated soil moisture. Correspondingly the 10%
 396 ASCAT soil moisture error standard deviation is also locally scaled by the ratio of the Noah

397 LSM and ASCAT soil moisture time series standard deviations following Draper et al. (2012)
398 and Jun et al. (2021). Unlike ASCAT, the SMAP soil moisture data are provided in the same
399 unit as the Noah LSM soil moisture, and only the climatological mean biases between the
400 SMAP soil moisture and modeled soil moisture are corrected during the bias correction
401 procedure (see Section 3.3). Therefore, the observation error standard deviation of SMAP is
402 not scaled in this study.

403 Note that there is a mismatch in the surface soil layer depth between the soil moisture
404 observations (i.e., 0–2 cm for ASCAT and 0–5 cm for SMAP) and Noah LSM (i.e., 0–10 cm).
405 However, Shellito et al. (2016, 2018) and Nair and Indu (2019) have demonstrated that
406 changing the surface layer depth in the model from 10 cm to 2 cm or 5 cm has only a
407 marginal impact on the simulated soil moisture. Moreover, because we apply the systematic
408 bias correction of the soil moisture retrievals before assimilation, the impact of the surface
409 soil layer depth difference on the DA performance is assumed to be negligible.

410

411 **5. Experiments**

412 Land-atmosphere coupled DA experiments (with a 6-hour cycling frequency) using the
413 active radar (i.e., ASCAT) and passive radiometer (i.e., SMAP) soil moisture retrievals are
414 designed as summarized in Table 2. CTL, a control case serving as a baseline experiment,
415 only assimilates atmospheric observations while an open-loop ensemble simulation of the
416 Noah LSM is performed without soil moisture assimilation. SG_AT and SG_SP are single-
417 sensor soil moisture DA experiments where the near-surface soil moisture data from
418 individual sensors (ASCAT or SMAP, respectively) are assimilated into the Noah LSM using

419 the 1-dimensional EnKF with an ensemble size of 20. MT_ATSP, a multi-sensor soil
 420 moisture DA experiment, jointly assimilates both ASCAT and SMAP soil moisture products
 421 to investigate the synergistic impact of assimilating the radar- and radiometer-based soil
 422 moisture retrievals together on improving the atmospheric analysis/forecast of the KIM-LIS
 423 coupled system. As explained in Section 3.3, the CDF matching and anomaly correction
 424 methods are applied for bias correction of the ASCAT and SMAP soil moisture retrievals,
 425 respectively, in the single- and multi-sensor soil moisture DA experiments. Atmospheric DA
 426 is performed identically in all experiments.

427
 428 **Table 2.** Summary of land-atmosphere coupled data assimilation (DA) experiments
 429 conducted in this study (SM: soil moisture; see Appendix A for additional abbreviations).

	CTL*	SG_AT	SG_SP*	MT_ATSP
<u>Land</u>				
SM DA	X	O	O	O
SM data	-	ASCAT	SMAP	ASCAT + SMAP
SM bias correction method	-	CDF matching	anomaly correction	CDF matching (ASCAT); anomaly correction (SMAP)
SM DA scheme	-	EnKF	EnKF	EnKF
LSM	Noah LSM v2.7.1 (KIM-LSM) and v3.3 (LIS-LSM)			
LSM horizontal resolution	25 km			
LSM ensemble size	20			
<u>Atmosphere</u>				
KIM	KIM v3.9			
KIM horizontal resolution	deterministic component (25 km); ensemble component (50 km)			
Atmospheric DA scheme	deterministic component (4DEnVar); ensemble component (LETKF)			
KIM ensemble size	50			
Experimental period	April 1 to July 31, 2022 (DA spin-up: March 1 to 31, 2022)			

430 *Note that CTL and SG_SP are the same experiments as those presented in Kwon et al.
 431 (2024).
 432

433 This study uses the same model setup and experimental period as in Kwon et al. (2024).
434 We use the Shuttle Radar Topography Mission (SRTM) elevation (Farr et al., 2007),
435 MODIS-IGBP land cover (Friedl et al., 2002), National Centers for Environmental Prediction
436 (NCEP) green vegetation fraction and surface albedo, and the blended State Soil Geographic
437 (STATSGO, Miller and White, 1998)/Food and Agriculture Organization (FAO) soil texture
438 (Reynolds et al., 2000) as land inputs for the Noah LSM. The LSM and KIM deterministic
439 component are run over the global domain at a horizontal resolution of 25 km while the KIM
440 ensemble component is run at a 50 km horizontal resolution due to its high computational
441 cost in the 6-hourly cycling experiments. All 6-hourly cycling experiments are conducted
442 from March to July 2022 while the first month is excluded from evaluation as it is used as the
443 assimilation spin-up (burn-in) period. To obtain LSM initial conditions at the beginning of
444 the experiments (i.e., March 1, 2022), an offline spin-up of the Noah LSM is first run from
445 2008 to April 2020 forced by the meteorological forcing fields from the Global Land Data
446 Assimilation System (GLDAS, Rodell et al., 2004), followed by additional spin-up until
447 March 1, 2022 using the KIM atmospheric forcing, which is available only from May 2020
448 for the LSM offline simulation. The KIM atmospheric model is initialized by the fifth
449 generation of the European Centre for Medium-Range Weather Forecasts (ECMWF)
450 atmospheric reanalysis (ERA5, Hersbach et al., 2020). In addition to the cycling runs in each
451 experimental case, 5-day forecasts are performed every 00 UTC and 12 UTC cycle after
452 being initialized by the land and atmospheric analyses from DA.

453

454

455 **6. Performance evaluation**

456 Due to the difficulty in acquiring a global ground truth reference dataset, we perform
457 global-scale performance evaluations of the soil moisture DA for different
458 hydrometeorological variables using datasets from various sources such as satellite-based
459 observations and analysis fields from different systems. The four experiments (i.e., CTL,
460 SG_AT, SG_SP, and MT_ATSP) listed in Table 2 are assessed in terms of generating the soil
461 moisture analysis, specific humidity and air temperature analyses/forecasts, and precipitation
462 forecasts. Methodologies and datasets employed in this study for the evaluation are described
463 below.

464

465 **6.1. Soil moisture**

466 A triple collocation analysis (TCA, Stoffelen, 1998; Scipal et al., 2008), a statistical
467 random error estimation method, is applied to evaluate the global soil moisture analysis from
468 the soil moisture DA experiments. TCA has been initially proposed by Stoffelen (1998) to
469 quantify the error of near-surface ocean wind speed estimates, and it is now one of the most
470 commonly used method for estimating uncertainties in satellite-based soil moisture retrievals
471 (e.g., Dorigo et al., 2010; Gruber et al., 2016; Kim et al., 2021b, 2023; Scipal et al., 2008) or
472 for evaluating large-scale soil moisture simulations of computational models (e.g., Kim et al.,
473 2021a; Kwon et al., 2024; Nair and Indu, 2019; Renzullo et al., 2014) due to no requirement
474 of reliable ground truth reference data that is hard to be obtained at large scales.

475 The TCA approach is based on the assumption of a linear relationship between
 476 hypothetical true soil moisture and individual soil moisture estimates as expressed in
 477 Equation (1):

$$478 \theta_k = \alpha_k + \beta_k \theta_{true} + \varepsilon_k \quad (1)$$

480
 481 where θ_k is independent collocated soil moisture datasets (i.e., triplet components, $k \in [x, y,$
 482 $z]$); α_k and β_k are additive and multiplicative systematic biases of θ_k , respectively, with
 483 respect to the unknown hypothetical true soil moisture signal (θ_{true}); and ε_k represents the
 484 additive random noise in each soil moisture data (θ_k). The random error (noise) variance ($\sigma_{\varepsilon_k}^2$)
 485 of three collocated soil moisture triplets [Equations (2) to (4)] can be derived from variance
 486 and covariance equations by introducing additional assumptions, i.e., error orthogonality
 487 (independence between the random error of the soil moisture datasets and the unknown soil
 488 moisture truth) and zero error-cross correlation (independence of the random errors between
 489 the soil moisture datasets) (Gruber et al., 2016).

$$490 \sigma_{\varepsilon_x}^2 = \sigma_x^2 - \frac{\sigma_{xy}\sigma_{xz}}{\sigma_{yz}} \quad (2)$$

$$491 \sigma_{\varepsilon_y}^2 = \sigma_y^2 - \frac{\sigma_{yx}\sigma_{yz}}{\sigma_{xz}} \quad (3)$$

$$492 \sigma_{\varepsilon_z}^2 = \sigma_z^2 - \frac{\sigma_{zx}\sigma_{zy}}{\sigma_{xy}} \quad (4)$$

496 where σ_k^2 and $\sigma_{\varepsilon_k}^2$ ($k \in [x, y, z]$) are the variance and random error variance, respectively, of
497 each soil moisture data; and σ_{xy} , σ_{xz} , and σ_{yz} are the covariances of two soil moisture
498 triplet components. In this study, the fractional mean-square error ($fMSE_k$, Draper et al.,
499 2013), ranging from 0 (free-of-noise soil moisture data) to 1 (no meaningful soil moisture
500 signal), is computed using Equation (5). This metric is employed as a TCA-based global soil
501 moisture evaluation measure, following procedures implemented by Kim et al. (2020 and
502 2021a) and Kwon et al. (2024).

503

$$504 \quad fMSE_k = \frac{\sigma_{\varepsilon_k}^2}{\sigma_k^2} \quad (5)$$

505

506 In order to meet the zero error-cross correlation assumption, we select two independent
507 satellite-based soil moisture products, i.e., ASCAT and Advanced Microwave Scanning
508 Radiometer 2 (AMSR2) [or Soil Moisture and Ocean Salinity (SMOS)], derived from
509 different microwave sensors using different retrieval algorithms for the first and second soil
510 moisture triplet components while the soil moisture simulations from the experiments (CTL,
511 SG_AT, and SG_SP) are used for the third triplet component (Table 3). Due to the TCA
512 assumptions, it is hard to compose the same reference frame for all experimental cases,
513 especially for the multi-sensor soil moisture DA experiment. Therefore, for a fair comparison,
514 we only evaluate the relative improvement in the soil moisture estimates by comparing fMSE
515 of the single-sensor soil moisture DA with fMSE of CTL that are computed using the same
516 first and second triplet components (i.e., satellite soil moisture retrievals that are not

517 assimilated in the soil moisture DA experiment) as shown in Table 3. The effects of the
 518 multi-sensor soil moisture DA (MT_ATSP) are assessed only for atmospheric variables (see
 519 Sections 6.2 and 6.3).

520

521 **Table 3.** Triple collocation analysis (TCA) triplet composition to quantify the relative
 522 improvement in the soil moisture estimates by soil moisture data assimilation (DA) as
 523 compared to CTL. The CTL soil moisture estimates are also evaluated using the same
 524 satellite-based reference soil moisture products as used for each single-sensor soil moisture
 525 DA experiment (EXP: SG_AT and SG_SP).

Experiments	Triples for EXP	Triples for CTL
SG_AT	AMSR2, SMOS, SG_AT	AMSR2, SMOS, CTL
SG_SP	AMSR2, ASCAT, SG_SP	AMSR2, ASCAT, CTL

526

527 The ASCAT, SMOS, and AMSR2 soil moisture data used in TCA are the 12.5-km
 528 ASCAT soil moisture Climate Data Record (CDR) version 7 product (H119 and extended
 529 H120) based on the TU-Wien change detection algorithm (Wagner et al., 2013), the SMOS-
 530 INRA-CESBIO (SMOS-IC) version 2 product, and the AMSR2 X-band Land Parameter
 531 Retrieval Model (LPRM) product, respectively. The original datasets are preprocessed by
 532 conducting quality control based on quality flags provided in each data product, and spatial
 533 resampling using the nearest neighbor distance method to match the spatial resolution of the
 534 datasets with that of the LSM outputs (i.e., 25-km latitude-longitude grids). Due to the
 535 different local overpass time between the satellite soil moisture products [i.e., 09:30 am/pm
 536 LST for ASCAT, 01:30 am/pm LST for ASMR2, and 06:00 am/pm LST for SMOS], the
 537 UTC-based Noah-LSM outputs at 04:00 am/pm LST and 11 am/pm LST are extracted for
 538 TCA that uses AMSR2/SMOS/SG_AT(or CTL) and AMSR2/ASCAT/SG_SP(or CTL),
 539 respectively. We select model outputs at the approximate midpoint time (e.g., 04:00) between

540 the overpass times of two other satellite-based soil moisture triplet components (e.g., 01:30
541 AMSR2 and 06:00 SMOS) for a fair comparison. While some errors may still arise due to
542 sampling-time mismatches between the triplet components, we assume these errors are
543 acceptable since the same sampling time was applied to both CTL and DA experimental
544 outputs to evaluate their relative performance. Please refer to Kwon et al. (2024) and Kim et
545 al. (2023) for more detailed procedures.

546

547 **6.2. Specific humidity and air temperature**

548 Evaluations of the specific humidity and air temperature analyses/forecasts are performed
549 using the ECMWF Integrated Forecasting System (IFS) analysis (ECMWF, 2017) as
550 reference data, which has been extensively used for evaluating modeling systems (e.g., Ben
551 Bouallègue et al., 2024; Kwon et al., 2024; Lee et al., 2020; Polichtchouk et al., 2023;
552 Reichle et al., 2023). The root mean square difference (RMSD) between the atmospheric
553 variables (i.e., specific humidity and air temperature) from each experiment and those from
554 the IFS analysis is computed.

555

556 **6.3. Precipitation**

557 Local variations in soil moisture modify boundary-layer heat and moisture fluxes, thereby
558 altering water–energy budgets and influencing convective triggering (Findell and Eltahir,
559 2003; Pal and Eltahir, 2003) and subsequently influence large-scale dynamics (Cook et al.,
560 2006; Pal and Eltahir, 2003), both of which play key roles in determining precipitation
561 processes. A number of studies have investigated the complex interaction mechanisms

562 between soil moisture and precipitation, referred to as the ‘soil moisture-precipitation
563 feedback’, using observational analyses (e.g., Catalano et al., 2016; Yang et al., 2018) and
564 computational modeling systems (e.g., Beljaars et al., 1996; Bosilovich and Sun, 1999;
565 Hohenegger et al., 2009; Lin et al., 2023; Pal and Eltahir, 2003). Although these studies
566 generally agree on a predominant positive feedback, the sign and strength vary depending on
567 modeling systems and spatiotemporal scales (Hohenegger et al., 2009; Lin et al., 2023).
568 Differences in the sign of soil moisture-precipitation feedback can be attributed to the
569 complexity of representing the soil moisture-evapotranspiration relationship (Yang et al.,
570 2018) and convective development (Hohenegger et al., 2009). Considerable debate and
571 uncertainty remain regarding the physical mechanisms determining the sign of the feedback
572 (Hohenegger et al., 2009). Nevertheless, there is no doubt that soil moisture and precipitation
573 are reciprocally linked, implying that better characterization of soil moisture conditions
574 through soil moisture DA can enhance precipitation forecasts in land-atmosphere coupled
575 systems.

576 We assess the impact of soil moisture DA on precipitation forecast skill using well-
577 established metrics, such as the frequency bias (FB) and equitable threat score (ETS) based
578 on recommendations by the World Meteorological Organization (WMO, 2008). Calculations
579 of the FB and ETS metrics are based on a 2×2 contingency table (Table 4), which consists
580 of *Hits*, *Misses*, *FalseAlarms*, and *CorrectNegatives*. Gauge-based global daily precipitation
581 analyses from the National Oceanic and Atmospheric Administration (NOAA) Climate
582 Prediction Center (CPC) (Chen et al., 2008; Xie et al., 2007) are used as reference data for
583 precipitation evaluation.

584 **Table 4.** Contingency table for computing precipitation forecast evaluation metrics

		Observation (reference data)	
		Yes	No
Forecast (model data)	Yes	<i>Hits</i>	<i>FalseAlarms</i>
	No	<i>Misses</i>	<i>CorrectNegatives</i>

585

586 FB [Equation (6)] assesses the ratio of the frequency of precipitation occurrence in the
587 forecast to that in the observation:

588

$$589 \quad FB = \frac{Hits + FalseAlarms}{Hits + Misses} \quad (6)$$

590

591 where *Hits*, *FalseAlarms*, and *Misses* are the number of model grid points with correct
592 forecasts, false alarms, and missed forecasts of precipitation occurrence, respectively. The FB
593 metric ranges from zero to infinity where the ideal FB score is 1.0, indicating that the number
594 of the forecasted precipitation events is the same as that of the observed events. Note that FB
595 does not consider the timing of precipitation events.

596 ETS [Equation (7)] quantifies the fraction of the forecasted or observed precipitation
597 events that are captured correctly after excluding random hits (*Hits_{rnd}*), which is the number
598 of correct forecasts by random chance computed using Equation (8):

599

$$600 \quad ETS = \frac{Hits - Hits_{rnd}}{Hits + Misses + FalseAlarms - Hits_{rnd}} \quad (7)$$

601

$$602 \quad Hits_{rnd} = \frac{(Hits + Misses)(Hits + FalseAlarms)}{N} \quad (8)$$

603 where N is the total number of events defined as $N = Hits + Misses + FalseAlarms +$
604 $CorrectNegatives$. $CorrectNegatives$ denotes the number of correct forecasts of no
605 precipitation. The ETS metric ranges from $-1/3$ to 1, where values below 0 and 1 represent
606 “no skill” and “perfect skill” (no $Misses$ or $FalseAlarms$), respectively.

607

608 **7. Results**

609 In this section, we first examine the performance of the KIM-LIS coupled system in
610 producing enhanced global soil moisture estimates when the system is informed by satellite-
611 based soil moisture retrievals from ASCAT and SMAP via assimilation. Next, the impacts of
612 assimilating the ASCAT and SMAP soil moisture data, both individually and simultaneously,
613 on atmospheric analyses and forecasts are assessed. Finally, we evaluate the added skill of the
614 KIM-LIS system in forecasting precipitation when using initialized soil moisture conditions
615 from multi-sensor soil moisture DA.

616

617 **7.1. Soil moisture analysis**

618 The impact of single-sensor soil moisture assimilation (i.e., SG_AT and SG_SP) on the
619 global soil moisture estimates is evaluated using the TCA method (see Section 6.1). Figure 2
620 presents the spatial distribution of fMSE obtained from TCA during the experimental period
621 from April to July 2022. Both ASCAT and SMAP are seen to have an overall positive impact
622 on the surface soil moisture estimates of the Noah LSM through assimilation. Compared to
623 the CTL experiment, which does not assimilate soil moisture data, SG_AT and SG_SP
624 reduce the global mean fMSE by 4.0% (Figure 2a) and 10.5% (Figure 2b), respectively. In

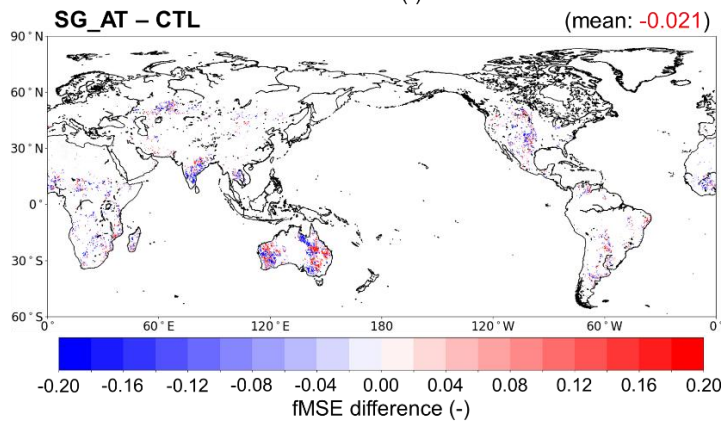
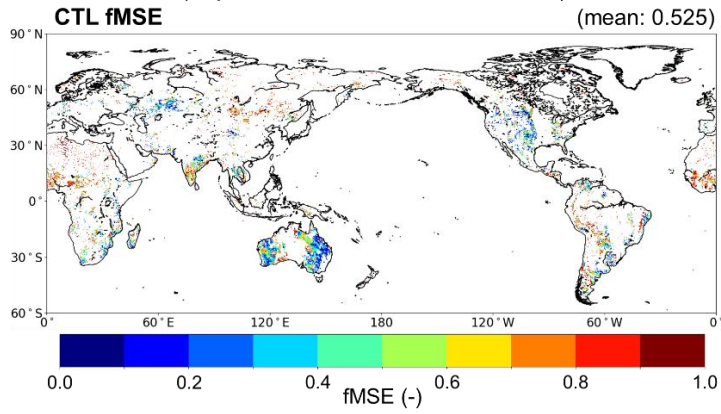
625 both single-sensor soil moisture DA cases, obvious improvements in soil moisture are
626 observed in Asia while a decrease in skill is mostly found in the Australian and North
627 American continents where CTL already exhibits a relatively good performance in estimating
628 soil moisture.

629 Note that we use identical first and second triplet components for DA and CTL (Table 3),
630 replacing only the CTL soil moisture estimates with those from the DA experiments (SG_AT
631 and SG_SP) to assess the relative performance gain from soil moisture DA. This approach
632 (i.e., replacing one triplet member) may alter the fMSE calculation of the other two triplet
633 components and thus influence the comparison results between DA and CTL. However,
634 because the soil moisture estimates from DA and CTL share the same spatial and temporal
635 coverage and climatology, as they are generated from the identical modeling system, the
636 impact of replacing the model-based triplet member is negligible, as shown in Figure S1.
637 Therefore, the fMSE comparison results (Figure 2) can be considered reliable.

638

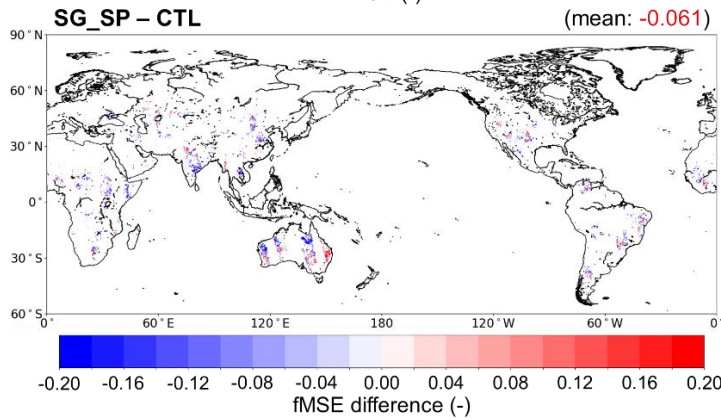
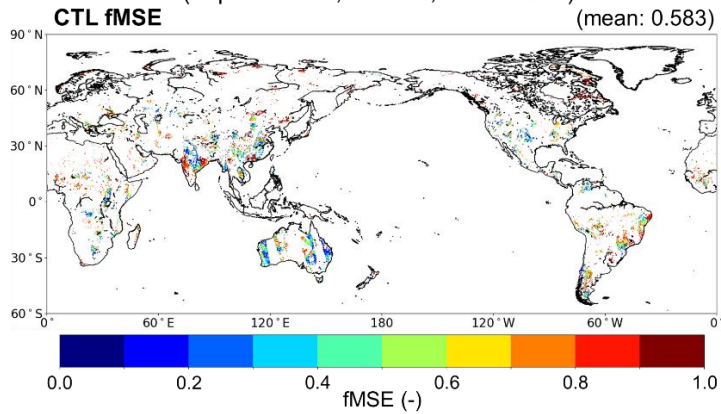
a) Evaluation of ASCAT SM DA

(Triplet: model, AMSR2, and SMOS)



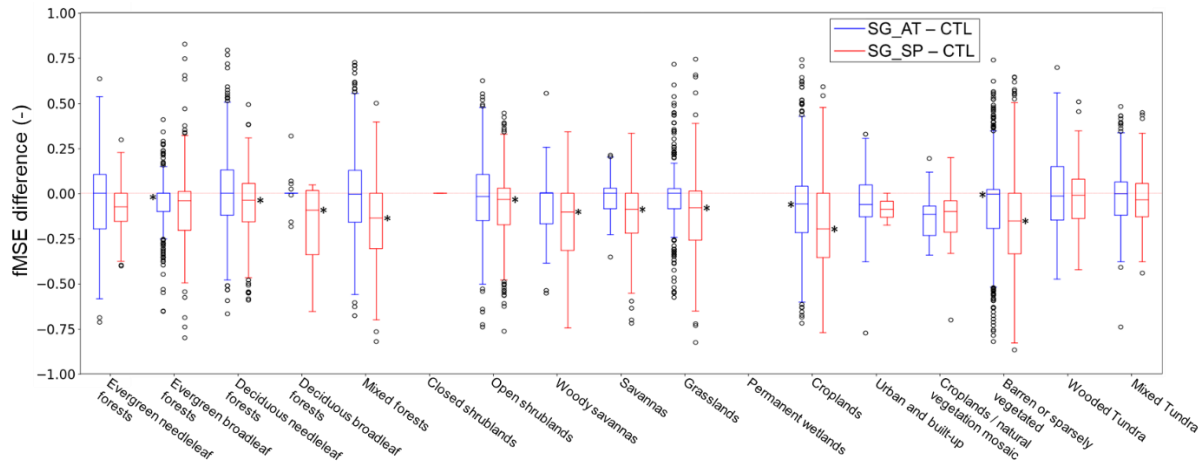
b) Evaluation of SMAP SM DA

(Triplet: model, AMSR2, and ASCAT)



640 **Figure 2.** Global maps of the soil moisture triple collocation analysis (TCA) results for (a)
641 ASCAT (i.e., SG_AT) and (b) SMAP soil moisture data assimilation (i.e., SG_SP). In each
642 panel, the top subpanel shows the fractional mean-square error (fMSE) of CTL soil moisture
643 at 04:00 am/pm local solar time (LST) in (a) and 11:00 am/pm LST in (b). The bottom
644 subpanel shows the soil moisture fMSE difference between SG_AT and CTL in (a) and
645 between SG_SP and CTL in (b). Negative fMSE differences indicate improved soil moisture
646 estimates from ASCAT and SMAP data assimilation, respectively.
647

648 Because land surface characteristics affect the soil moisture skill of models and
649 observations (Draper et al., 2012), the TCA results are also plotted for the MODIS-IGBP land
650 cover types. Figure 3 shows that for all land cover types, both SG_AT and SG_SP enhance
651 the skill of the modeled soil moisture relative to CTL in terms of the median fMSE, with
652 SG_SP achieving greater skill gains. The soil moisture estimates are significantly improved
653 by SG_AT for evergreen broadleaf forests and croplands, and by SG_SP for deciduous
654 needleleaf forests, deciduous broadleaf forests, mixed forests, open shrublands, woody
655 savannas, savannas, grasslands, croplands, and barren or sparsely vegetated land cover types.
656 In both SG_AT and SG_SP experiments, the highest skill improvements, in terms of the
657 median fMSE, are observed for croplands. This implies that the land DA system effectively
658 utilizes soil moisture signals related to agricultural practices from satellite observations,
659 especially in the case of SMAP soil moisture DA (SG_SP), which employs the anomaly-
660 based bias correction approach.
661



662 **Figure 3.** Differences in the soil moisture fractional mean-square error (fMSE) between the
 663 single-sensor soil moisture data assimilation (i.e., SG_AT and SG_SP) and control [without
 664 soil moisture data assimilation (DA); i.e., CTL] experiments depending on land cover types.
 665 A dominant land cover type in each model grid is obtained from the MODIS-IGBP land
 666 cover classifications (Friedl et al., 2002). The asterisk symbol (*) indicates statistical
 667 significance at $p < 0.05$. Negative values represent the improved soil moisture estimates by
 668 soil moisture DA. Results are not plotted for closed shrublands and permanent wetlands
 669 because of missing triplet data.
 670
 671

672 Figures 2 and 3 indicate that SMAP DA shows higher skill than ASCAT DA for the soil
 673 moisture analysis. The superior performance of SMAP over ASCAT within a land DA
 674 system is also reported in Seo et al. (2021) where SMAP and ASCAT soil moisture DA
 675 results are evaluated against *in situ* measurements in the continental United States. These
 676 results can be supported by the fact that L-band brightness temperature measurements have
 677 higher sensitivity to soil moisture variations than C-band backscatter measurements (Kolassa
 678 et al., 2017), and thus the SMAP soil moisture retrievals have better accuracy (Al-Yaari et al.,
 679 2019; Kumar et al., 2018). However, note that in this study, a direct comparison of the global
 680 soil moisture analysis between SG_AT and SG_SP is not made because the model soil
 681 moisture outputs used in TCA are extracted at different LST—specifically, 04:00 am/pm for

682 SG_AT and 11:00 am/pm for SG_SP—due to the different local overpass times of the
683 satellite soil moisture data used for TCA-based assessment (see Section 6.1).

684 As shown in Figure 2, soil moisture performance gains and losses by each single-sensor
685 soil moisture DA are locally dependent. Thus, some previous studies (e.g., Draper et al., 2012;
686 Kolassa et al., 2017) have shown that simultaneously assimilating soil moisture retrievals
687 from both passive and active sensors achieves higher model soil moisture accuracy than
688 assimilating a single product. However, because soil moisture triplets that fully satisfy the
689 TCA assumptions (see Section 6.1) are difficult to obtain over the global domain for the
690 multi-sensor soil moisture DA experiment, the combined effects of ASCAT and SMAP DA
691 are discussed only in terms of atmospheric variables, which are the ultimate objective of this
692 study, in the subsequent sections.

693

694 **7.2. Analysis and forecast of specific humidity and air temperature**

695 Domain-averaged RMSD differences (i.e., RMSD_{EXP} minus RMSD_{CTL}) in the specific
696 humidity analysis (Figures 4a to 4c) and air temperature analysis (Figures 4d to 4f) are
697 evaluated across atmospheric levels and over time. Compared to CTL (without soil moisture
698 DA), ASCAT DA (i.e., SG_AT) has more beneficial impacts on the air temperature analysis
699 (Figure 4d) while SMAP DA (i.e., SG_SP) has more beneficial impacts on the specific
700 humidity analysis (Figure 4b). Figures 4c and 4f show that the simultaneous assimilation of
701 ASCAT and SMAP soil moisture retrievals (i.e., MT_ATSP) improves the analysis of both
702 atmospheric variables relative to CTL. Notably, degradations in the specific humidity and air

703 temperature analyses by SG_AT and SG_SP, respectively, are compensated by additionally
704 assimilating other soil moisture products.

705 Figure 5 more clearly demonstrates that multi-sensor soil moisture DA enhances the
706 performance of the specific humidity (Figure 5a) and air temperature analyses (Figure 5d)
707 compared to the single-sensor soil moisture DA cases (i.e., SG_AT and SG_SP, respectively).
708 Although MT_ATSP exhibits somewhat reduced performance in the air temperature (Figure
709 5c) and specific humidity analyses (Figure 5b) compared to SG_AT and SG_SP, respectively,
710 it achieves a more balanced improvement, meaning that neither variable is degraded while
711 both show moderate gains compared to CTL, by assimilating radar- and radiometer-based
712 soil moisture data together.

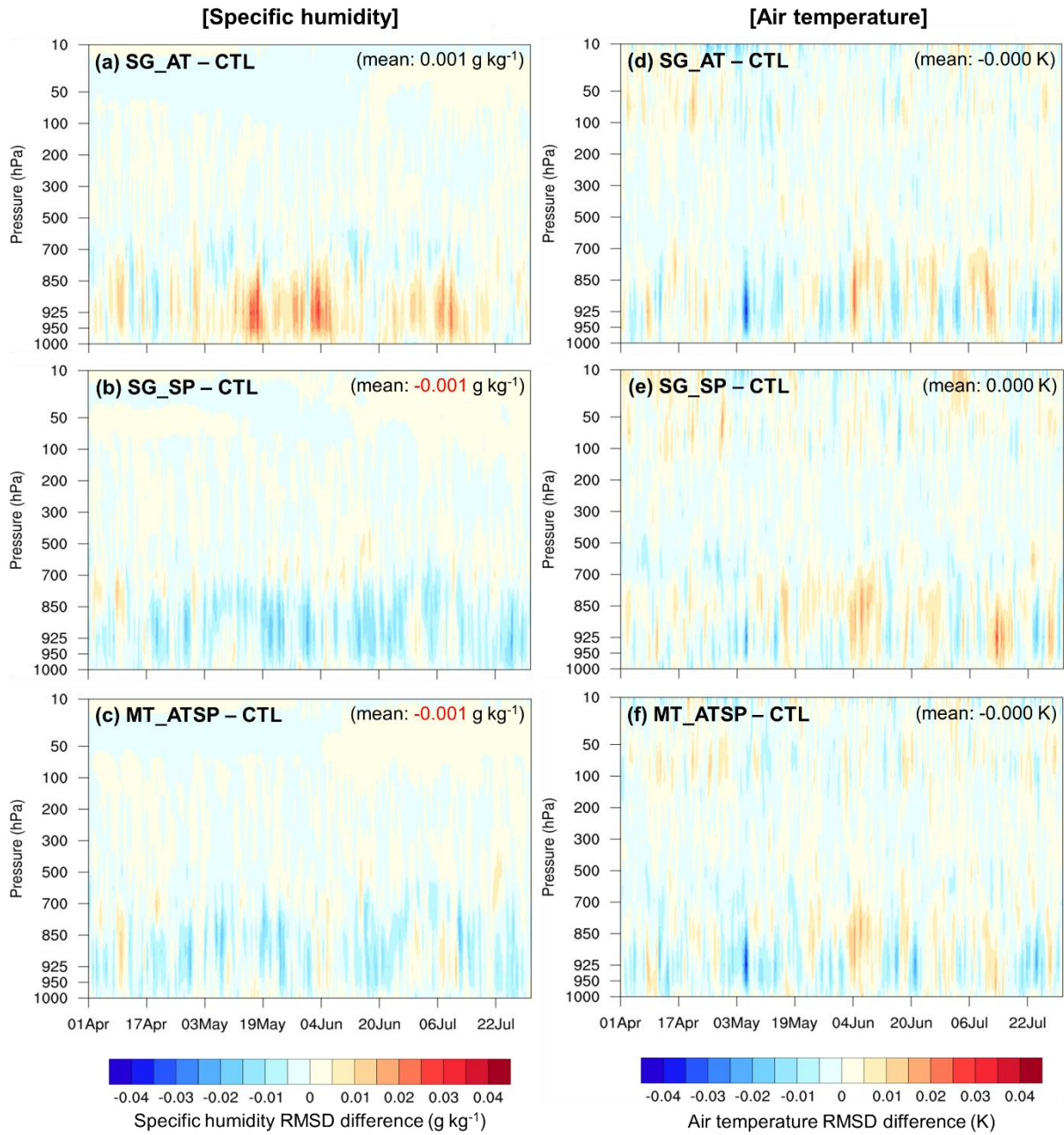
713 Tables 5 and 6 summarize the domain-averaged RMSD differences between the soil
714 moisture DA experiments and CTL for the analyses and forecasts of 2-m atmospheric
715 variables (i.e., specific humidity and air temperature) from the 00 UTC cycle (Table 5) and
716 the 12 UTC cycle (Table 6). In the global domain, SG_SP generally achieves better domain-
717 averaged analysis and forecast skills for both 2-m atmospheric variables compared to SG_AT
718 (Tables 5 and 6), except for the 2-m air temperature forecast of the 12 UTC cycle, where
719 SG_AT performs slightly better (Table 6). During the experimental period, all soil moisture
720 DA cases are more effective in improving the 2-m air temperature analysis and forecast than
721 those of specific humidity, especially for the 00 UTC cycle. Overall, they perform better in
722 the Northern Hemisphere than in the Southern Hemisphere (Tables 5 and 6), although they
723 achieve greater 2-m air temperature forecast skill during the 00 UTC cycle in the Southern
724 Hemisphere (Table 5). The lower analysis and forecast skills of soil moisture DA in the

725 Southern Hemisphere can be attributed to the use of spatially and temporally constant
726 observations errors (see Section 4.2), which do not adequately reflect the relatively higher
727 uncertainties in winter-period soil moisture data.

728 For the 2-m specific humidity estimates, the assimilation of SMAP soil moisture
729 retrievals alone (SG_SP) achieves the best domain-averaged performance (Tables 5 and 6).
730 MT_ATSP reduces RMSD compared to SG_AT by additionally assimilating the SMAP soil
731 moisture data, but it exhibits relatively lower skill in specific humidity than SG_SP. However,
732 in Europe and tropical regions, MT_ATSP provides improved 2-m specific humidity
733 forecasts compared to SG_SP, particularly when both ASCAT and SMAP have a positive
734 impact. The synergistic impacts of the combined assimilation of ASCAT and SMAP are
735 evident in the 2-m air temperature analysis and forecast of the 00 UTC cycle (Table 5).
736

Atmospheric analysis RMSD difference (EXP – CTL)

(Evaluation period: April to July; Reference data: ECMWF-IFS analysis)

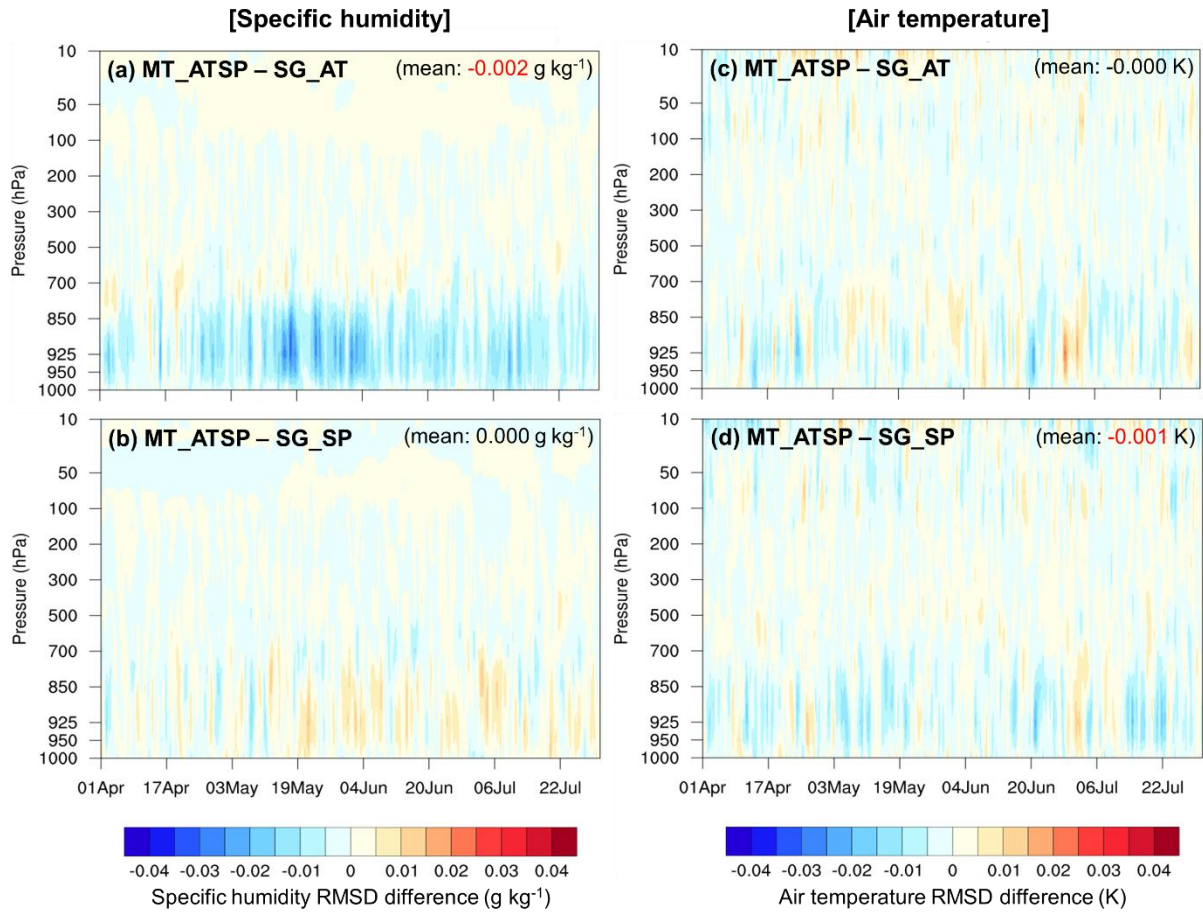


737
738
739
740
741
742
743

Figure 4. Vertical profile time series of RMSD differences in the specific humidity analysis (left column) and air temperature analysis (right column) between the soil moisture data assimilation (DA) and CTL experiments. The RMSD is calculated using the ECMWF-IFS analysis as reference data. Negative RMSD differences indicate improved estimates of the atmospheric variables by assimilating the soil moisture retrievals.

Atmospheric analysis RMSD difference (MT_ATSP – SG)

(Evaluation period: April to July; Reference data: ECMWF-IFS analysis)



744
745
746
747
748
749
750
751
752
753
754
755

Figure 5. Vertical profile time series of RMSD differences in the specific humidity analysis (left column) and air temperature analysis (right column) between the multi-sensor soil moisture data assimilation (DA) (MT_ATSP) and single- sensor soil moisture DA [SG_AT (a and c) and SG_SP (b and d)] experiments. The RMSD is calculated using the ECMWF-IFS analysis as reference data. Negative RMSD differences indicate improved estimates of the atmospheric variables by additionally assimilating the SMAP or ASCAT soil moisture retrievals.

756 **Table 5.** Domain-averaged RMSD differences ($\Delta\text{RMSD} = \text{RMSD}_{\text{EXP}} - \text{RMSD}_{\text{CTL}}$) for the 2-m specific humidity and air temperature analyses
757 and (5-day) forecasts across six domains [i.e., global domain (GLOB), Northern Hemisphere (NH), Southern Hemisphere (SH), Asia (ASIA),
758 Europe (EU), and tropical area (TROP)]. The RMSD is calculated for the 00 UTC cycle from April to July 2022 (whole experimental period)
759 using the ECMWF-IFS analysis as reference data. Negative ΔRMSD indicates improved estimates of the atmospheric variables by
760 assimilating the soil moisture retrievals.

April to July 2022 (00 UTC)				2-m specific humidity ΔRMSD (EXP – CTL) [g kg ⁻¹]														
Domain	Analysis			Forecast														
	SG_ AT	SG_ SP	MT_ ATSP	1-day lead time			2-day lead time			3-day lead time			4-day lead time			5-day lead time		
				SG_ AT	SG_ SP	MT_ ATSP	SG_ AT	SG_ SP	MT_ ATSP	SG_ AT	SG_ SP	MT_ ATSP	SG_ AT	SG_ SP	MT_ ATSP	SG_ AT	SG_ SP	MT_ ATSP
GLOB	0.011	-0.001	0.001	0.012	0.001	0.002	0.014	0.004	0.005	0.013	0.004	0.004	0.014	0.004	0.006	0.017	0.004	0.010
NH	0.005	-0.006	-0.005	0.005	-0.004	-0.004	0.006	-0.002	-0.001	0.006	-0.002	-0.001	0.005	-0.004	0.000	0.009	-0.005	0.001
SH	0.046	0.025	0.040	0.029	0.011	0.016	0.026	0.010	0.012	0.017	0.006	0.007	0.018	0.007	0.009	0.022	0.016	0.025
ASIA	0.004	-0.004	-0.002	0.003	-0.001	0.000	0.006	0.002	0.003	0.008	0.004	0.004	0.009	0.003	0.006	0.009	0.006	0.010
EU	0.016	-0.001	0.003	0.012	-0.002	-0.004	0.010	-0.000	-0.005	0.004	-0.001	-0.006	0.002	0.006	0.000	0.002	0.003	0.001
TROP	0.008	-0.001	-0.004	0.016	0.005	0.005	0.021	0.011	0.010	0.022	0.012	0.011	0.023	0.013	0.013	0.025	0.014	0.017

				2-m air temperature ΔRMSD (EXP – CTL) [K]														
Domain	Analysis			Forecast														
	SG_ AT	SG_ SP	MT_ ATSP	1-day lead time			2-day lead time			3-day lead time			4-day lead time			5-day lead time		
				SG_ AT	SG_ SP	MT_ ATSP	SG_ AT	SG_ SP	MT_ ATSP	SG_ AT	SG_ SP	MT_ ATSP	SG_ AT	SG_ SP	MT_ ATSP	SG_ AT	SG_ SP	MT_ ATSP
GLOB	0.001	0.000	-0.003	-0.000	-0.014	-0.013	0.001	-0.013	-0.011	0.001	-0.011	-0.010	0.003	-0.010	-0.008	0.005	-0.009	-0.003
NH	0.001	-0.008	-0.007	0.002	-0.005	-0.005	0.007	0.002	0.002	0.010	0.006	0.006	0.013	0.009	0.011	0.015	0.008	0.017
SH	0.016	0.002	-0.003	0.006	-0.012	-0.009	-0.006	-0.027	-0.022	-0.016	-0.028	-0.028	-0.019	-0.033	-0.029	-0.012	-0.021	-0.024
ASIA	-0.000	-0.007	-0.003	-0.001	-0.009	-0.025	-0.003	-0.009	-0.029	-0.003	-0.007	-0.029	0.002	-0.003	-0.020	0.005	-0.009	-0.015
EU	-0.005	-0.011	-0.010	-0.009	-0.033	-0.027	-0.001	-0.027	-0.019	-0.000	-0.026	-0.019	-0.003	-0.026	-0.019	-0.012	-0.038	-0.022
TROP	-0.005	0.012	0.001	-0.005	-0.027	-0.027	-0.006	-0.030	-0.028	-0.008	-0.032	-0.029	-0.007	-0.030	-0.029	-0.005	-0.030	-0.027

761
762
763
764

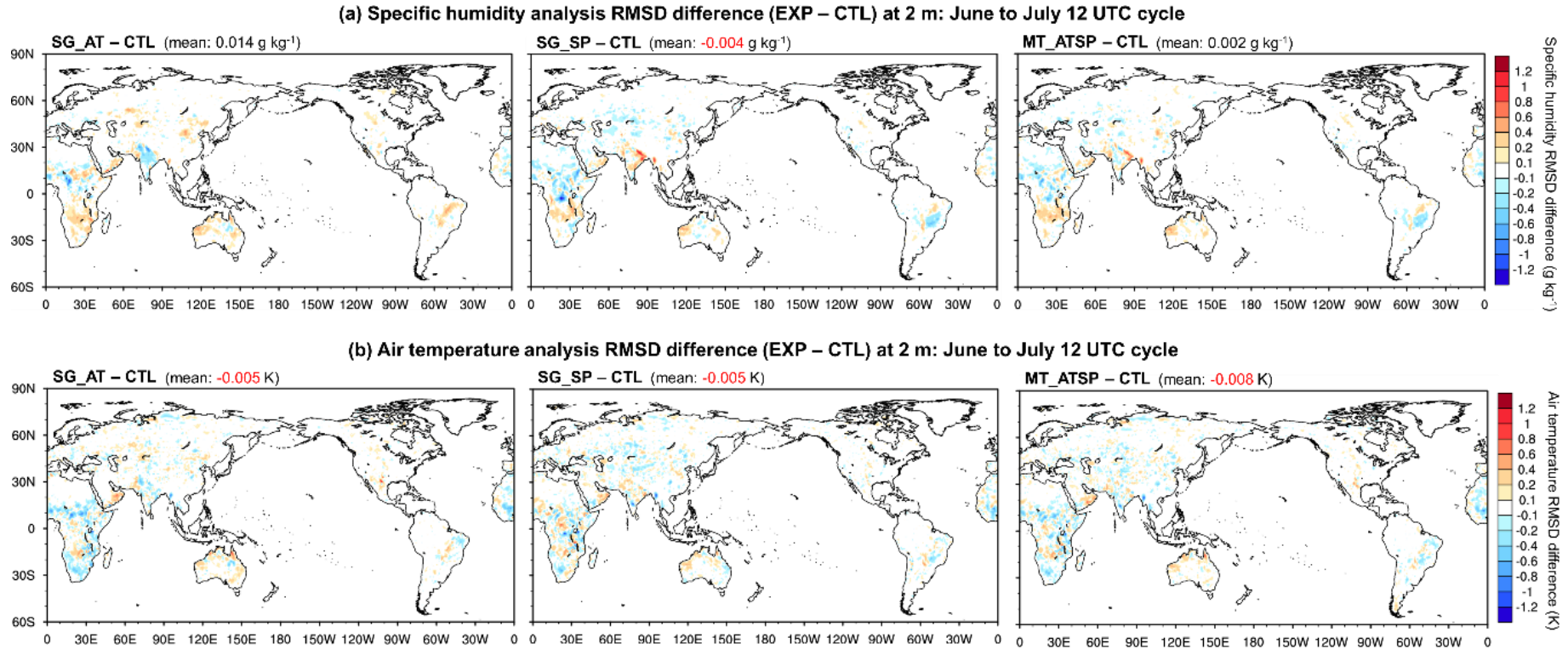
765 **Table 6.** Same as Table 5 but for the 12 UTC cycle from April to July 2022 (whole experimental period).

April to July 2022 (12 UTC)				2-m specific humidity Δ RMSD (EXP – CTL) [g kg ⁻¹]														
Domain	Analysis			Forecast														
	SG_ AT	SG_ SP	MT_ ATSP	1-day lead time			2-day lead time			3-day lead time			4-day lead time			5-day lead time		
				SG_ AT	SG_ SP	MT_ ATSP	SG_ AT	SG_ SP	MT_ ATSP	SG_ AT	SG_ SP	MT_ ATSP	SG_ AT	SG_ SP	MT_ ATSP	SG_ AT	SG_ SP	MT_ ATSP
GLOB	0.014	0.004	0.006	0.015	0.008	0.010	0.019	0.010	0.014	0.018	0.011	0.015	0.017	0.011	0.016	0.019	0.012	0.019
NH	0.003	-0.006	-0.005	0.005	-0.009	-0.006	0.007	-0.007	-0.001	0.006	-0.004	0.002	0.005	-0.004	0.002	0.008	-0.006	0.003
SH	0.052	0.026	0.036	0.064	0.040	0.050	0.060	0.033	0.045	0.053	0.029	0.041	0.046	0.027	0.042	0.046	0.030	0.046
ASIA	0.006	0.002	0.003	0.007	-0.002	0.001	0.011	-0.000	0.007	0.009	0.004	0.014	0.009	0.005	0.014	0.011	0.000	0.016
EU	-0.003	-0.007	-0.009	-0.003	-0.005	-0.009	-0.004	0.000	-0.007	-0.008	0.000	-0.008	-0.011	0.005	-0.005	-0.014	0.003	0.003
TROP	0.018	0.013	0.013	0.013	0.022	0.019	0.021	0.026	0.026	0.023	0.027	0.026	0.027	0.028	0.029	0.026	0.030	0.033

April to July 2022 (12 UTC)				2-m air temperature Δ RMSD (EXP – CTL) [K]														
Domain	Analysis			Forecast														
	SG_ AT	SG_ SP	MT_ ATSP	1-day lead time			2-day lead time			3-day lead time			4-day lead time			5-day lead time		
				SG_ AT	SG_ SP	MT_ ATSP	SG_ AT	SG_ SP	MT_ ATSP	SG_ AT	SG_ SP	MT_ ATSP	SG_ AT	SG_ SP	MT_ ATSP	SG_ AT	SG_ SP	MT_ ATSP
GLOB	-0.007	-0.010	-0.015	0.005	0.018	0.012	0.008	0.018	0.012	0.009	0.019	0.015	0.007	0.017	0.011	0.008	0.018	0.011
NH	0.002	-0.004	-0.007	-0.002	-0.008	-0.008	-0.000	-0.012	-0.009	-0.003	-0.015	-0.011	-0.004	-0.018	-0.018	-0.002	-0.018	-0.017
SH	0.008	-0.001	-0.004	0.070	0.037	0.051	0.082	0.045	0.060	0.087	0.050	0.071	0.091	0.060	0.079	0.082	0.056	0.073
ASIA	-0.006	-0.010	-0.018	0.002	-0.004	-0.002	0.011	-0.003	0.004	0.010	-0.007	0.004	0.009	-0.016	-0.006	0.015	-0.017	0.001
EU	0.000	-0.003	-0.000	-0.021	-0.004	-0.008	-0.026	-0.001	-0.011	-0.031	0.003	-0.015	-0.032	0.008	-0.020	-0.033	0.018	-0.009
TROP	-0.024	-0.021	-0.029	-0.007	0.049	0.026	-0.003	0.053	0.027	-0.000	0.058	0.033	-0.003	0.054	0.031	-0.000	0.058	0.031

766

767 Local performance differences in the 2-m atmospheric analysis between the single-sensor
768 soil moisture DA cases are clearly illustrated in Figure 6, which is plotted for the 12 UTC
769 cycle from June to July 2022. SG_AT and SG_SP exhibit opposite impacts on the
770 atmospheric analysis, especially on specific humidity, over India, Eurasia, and Brazil.
771 ASCAT DA (SG_AT) generally leads to the improved analyses of specific humidity and air
772 temperature over India while SMAP DA (SG_SP) performs better in Eurasia (except for
773 India and the southern part of West Asia) and Brazil. These discrepancies in the local
774 performance of 2-m specific humidity between ASCAT and SMAP DA may contribute to the
775 reduced domain-averaged skill of MT_ATSP relative to SG_SP, as shown in Tables 5 and 6.
776 In Africa, SG_AT yields better air temperature analysis than SG_SP, whereas SG_SP
777 outperforms SG_AT in the specific humidity analysis. It can be noted from Figure 6 that,
778 locally, the joint assimilation of the ASCAT and SMAP soil moisture retrievals yields the
779 best estimates of the 2-m atmospheric variables when both soil moisture products have
780 positive impacts.



781
782
783
784
785
786

Figure 6. Difference in the 2-m atmospheric analysis RMSD [i.e., specific humidity (upper panels) and air temperature (lower panels)] between the soil moisture data assimilation (DA) and CTL experiments. Evaluation results for the 12 UTC cycle from June to July 2022 (a two-month period) are presented with domain-averaged values in parenthesis. The RMSD is calculated using the ECMWF-IFS analysis as reference data. Negative RMSD differences indicate improved estimates of the atmospheric variables by assimilating the soil moisture retrievals.

787 7.3. Precipitation

788 The potential added value of multi-sensor soil moisture DA for precipitation forecasts is
789 assessed using categorical skill score metrics, including the FB and ETS, as detailed in
790 Section 6.3. Daily precipitation rates (mm day^{-1}) are computed from the KIM forecasts at 0-
791 24 h, 24-48 h, and 48-72 h lead times, and compared against reference data using seven
792 conventional thresholds (0.5, 1.0, 5.0, 10.0, 15.0, 20.0, and 25.0 mm day^{-1}). The numbers of
793 model grid points classified as *Hits*, *FalseAlarms*, *Misses*, and *CorrectNegatives* in the
794 contingency table (Table 4) are then counted, and FB and ETS are calculated for six domains
795 (i.e., global domain, Northern Hemisphere, Southern Hemisphere, Asia, Europe, and tropical
796 area). Figure S2 presents the FB and ETS of daily precipitation forecasts from KIM, averaged
797 over the three lead times, for CTL and the three soil moisture DA experiments (SG_AT,
798 SG_SP, and MT_ATSP) during the 00 UTC cycle in July 2022. The corresponding
799 differences ($\Delta\text{FB} = |\text{FB}_{\text{EXP}} - 1| - |\text{FB}_{\text{CTL}} - 1|$, $\Delta\text{ETS} = \text{ETS}_{\text{EXP}} - \text{ETS}_{\text{CTL}}$) are shown in
800 Figure 7.

801 In the global domain, CTL (without soil moisture DA) tends to overestimate precipitation
802 frequency ($\text{FB} > 1.0$), simulating excessive precipitation events, except for the precipitation
803 threshold of 25.0 mm day^{-1} (Figure S2a). The model significantly overestimates precipitation
804 at the 5.0 mm day^{-1} threshold and exhibits an FB close to 1 for heavier precipitation events
805 (20.0 and 25.0 mm day^{-1}) (Figure S2a), with regional variations (Figures S2b to S2f). Both
806 the smallest FB (close to 1.0) and the largest FB (> 2.5) are observed in the Southern
807 Hemisphere for the lightest (0.5 mm day^{-1}) and heaviest (25.0 mm day^{-1}) precipitation events,
808 respectively (Figure S2c).

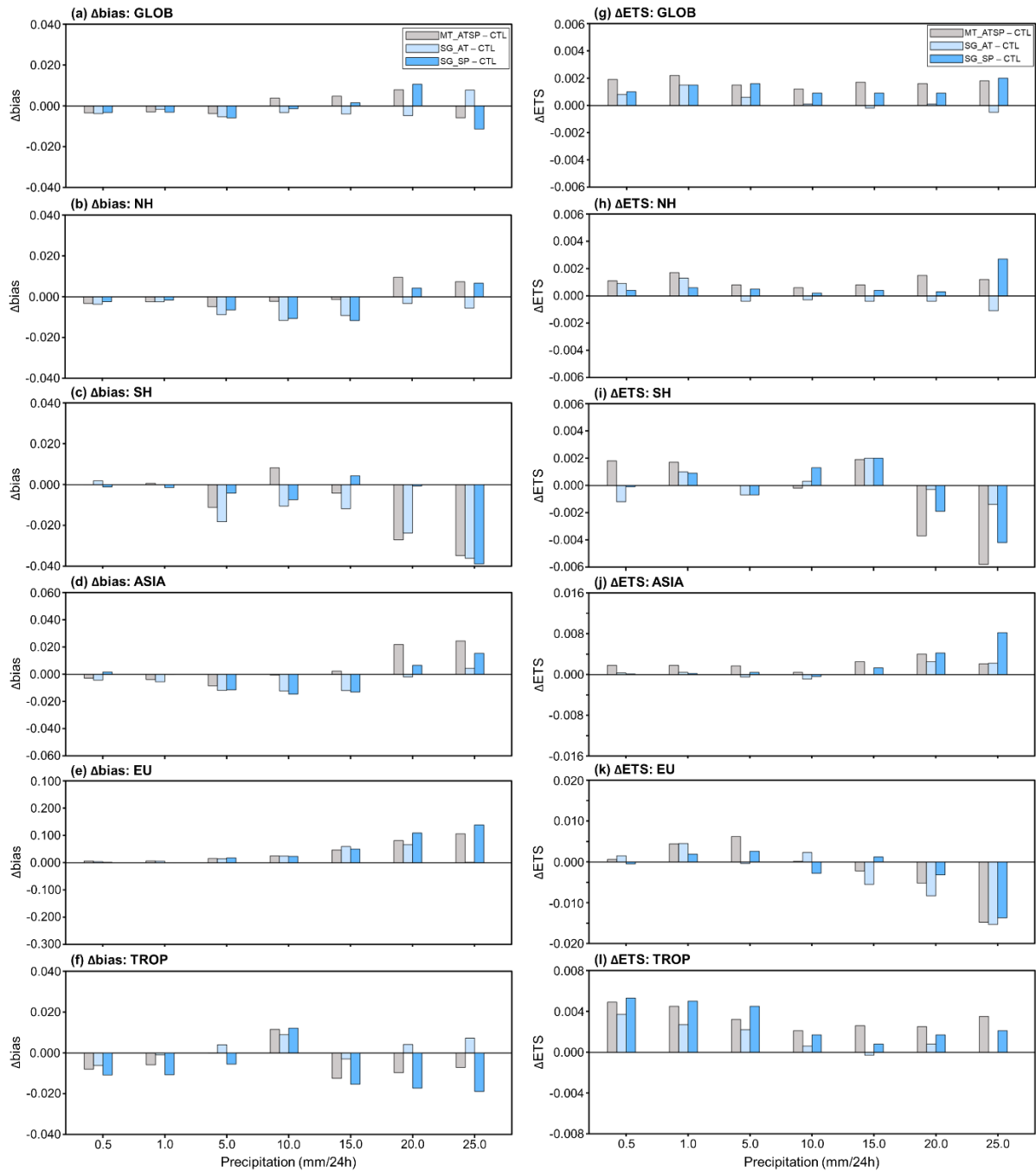
809 Unlike FB, ETS is higher (indicating better skill in predicting precipitation events) at
810 lower precipitation thresholds while ETS decreases as the precipitation intensity thresholds
811 increase in the global domain (Figure S2g) and in the Northern Hemisphere (Figure S2h),
812 including Asia (Figure S2j), Europe (Figure S2k), and tropical areas (Figure S2l). In the
813 Southern Hemisphere, CTL shows the highest ETS skill at the precipitation threshold of 10.0
814 mm day⁻¹ and the lowest at 1.0 mm day⁻¹ (Figure S2i). The different model performance
815 patterns (in both FB and ETS) between the Northern and Southern Hemispheres across the
816 range of precipitation intensity thresholds may be attributed to different weather regimes
817 associated with cyclones and monsoons (Dare and Ebert, 2017), along with additional
818 impacts from seasonal variations.

819 Overall, soil moisture DA improves the prediction of precipitation events (i.e., better ETS;
820 Figure 7g) while its contribution to precipitation frequency (FB) remains neutral (Figure 7a).
821 MT_ATSP demonstrates higher ETS skill than CTL (by up to 1.8%) and single-sensor soil
822 moisture DA (by up to 2.4% and 0.6% relative to SG_AT and SG_SP, respectively) (Figure
823 7g). The impacts of MT_ATSP on the global FB are marginal, showing negligible
824 improvements at the 0.5, 1.0, 5.0, and 25.0 mm day⁻¹ thresholds and slight overpredictions at
825 the 10.0, 15.0, and 20.0 mm day⁻¹ thresholds (Figure 7a, Figure S2a). Similar soil moisture
826 DA performance patterns are observed in the Northern Hemisphere (Figures 7b and 7h) and
827 Asia (Figures 7d and 7j). In the Southern Hemisphere, MT_ATSP slightly improves FB for
828 heavy precipitation events (precipitation thresholds ≥ 15.0 mm day⁻¹) while relatively
829 obvious improvements in ETS by MT_ATSP are witnessed at lower thresholds (≤ 1.0 mm
830 day⁻¹) (Figures 7c and 7i). Compared to CTL and SG_AT, multi-sensor soil moisture DA

831 enhances ETS across precipitation thresholds in tropical areas, although it is slightly less
832 effective than SG_SP at thresholds $\leq 5.0 \text{ mm day}^{-1}$ (Figure 7l). For FB, MT_ATSP shows
833 improvements over CTL and SG_AT in tropical areas, except at thresholds of 5.0 and 10.0
834 mm day^{-1} , where SG_SP performs better (Figure 7f). In contrast, MT_ATSP is generally
835 ineffective in Europe (Figures 7e and 7k), except for ETS at precipitation thresholds of 5.0
836 mm day^{-1} or lower. The overprediction of precipitation in Europe (Figure 7e, Figure S2e),
837 especially for heavy precipitation events ($\geq 15.0 \text{ mm day}^{-1}$), may lead to a decrease in ETS
838 (Figure 7k, Figure S2k).

839 The regional variability in precipitation performance between the CTL and soil moisture
840 DA experiments may be attributed to seasonality. A full-year or multi-year experiment would
841 therefore be valuable in future studies to assess the impact of seasonality on the effectiveness
842 of multi-sensor soil moisture DA for improving precipitation forecasts.

843



844
845
846
847
848
849
850

Figure 7. Differences in frequency bias ($\Delta FB = |FB_{EXP} - 1| - |FB_{CTL} - 1|$; a to f) and equitable threat score ($\Delta ETS = ETS_{EXP} - ETS_{CTL}$; g to l) between EXP (MT_ATSP, SG_AT, and SG_SP) and CTL, averaged over 24-72 h precipitation forecasts from the 00 UTC cycle in July 2022, for six domains [i.e., global domain (GLOB; a and g), Northern Hemisphere (NH; b and h), Southern Hemisphere (SH; c and i), Asia (ASIA; d and j), Europe (EU; e and k), and tropical area (TROP; f and l)]. The skill metrics are computed for seven conventional

851 thresholds (i.e., 0.5, 1.0, 5.0, 10.0, 15.0, 20.0, and 25.0 mm day⁻¹). Negative Δ FB and
852 positive Δ ETS values indicate improvements from soil moisture DA.
853

854 **8. Discussion**

855 **8.1. ASCAT data assimilation**

856 The experimental results indicate that SMAP DA slightly outperforms ASCAT DA in
857 enhancing near-surface atmospheric analyses and forecasts. While many factors may affect
858 the overall performance of each experiment, one factor may be related to errors resulting
859 from subsurface scattering, which are not accounted for in the ASCAT soil moisture data
860 used in this study, as discussed by Wagner et al. (2024). The current TU Wien change
861 detection algorithm (Wagner et al., 1999, 2010), used to retrieve soil moisture from ASCAT
862 backscatter observations, is based on the assumption of a positive linear relationship between
863 soil backscatter and wetness. However, Wagner et al. (2024) demonstrated that this
864 assumption fails when coarse fragments (e.g., stones and rocks) or discontinuities exist in the
865 soil profile, as they increase subsurface scattering contributions to total backscatter signals
866 under dry soil conditions. This eventually reverses the relationship between backscatter
867 signals and soil moisture content, deteriorating the quality of soil moisture data retrieved with
868 the current algorithm in many arid and semiarid regions. This phenomenon partly explains
869 why ASCAT DA exhibits better performance in croplands than in barren or sparsely
870 vegetated areas, as shown in Figure 3, which is consistent with results from soil moisture data
871 evaluation studies (e.g., Dorigo et al., 2010).

872 Soil moisture bias correction methods used to remove systematic discrepancies between
873 observations and models may also influence the ASCAT soil moisture DA performance.

874 Kumar et al. (2015) and Kwon et al. (2022, 2024) have shown that different bias correction
875 methods can substantially impact soil moisture DA performance. In SMAP DA, soil moisture
876 temporal variability information is directly assimilated (i.e., anomaly correction method). In
877 contrast, ASCAT DA employs the CDF matching method because it does not satisfy the
878 underlying assumption of the anomaly correction method (see Section 3.3). It is a known
879 issue that rescaling-based bias correction, such as CDF matching, causes a significant loss of
880 information (Kumar et al., 2015). Meanwhile, Text S2 and Figures S3-S5 suggest that
881 employing the anomaly correction method in soil moisture DA worsens the atmospheric
882 analysis within land-atmosphere coupled systems when the underlying assumptions of the
883 anomaly correction approach are not met. Rather than relying on CDF matching and anomaly
884 correction methods, a more robust and appropriate bias correction approach is required for
885 improving ASCAT soil moisture DA.

886

887 **8.2. Soil moisture observation error**

888 The effectiveness of the combined assimilation of multiple soil moisture products from
889 different sources (i.e., radar backscatter and radiometer brightness temperature observations)
890 in enhancing the soil moisture analysis skill has been demonstrated in previous studies (e.g.,
891 Blyverket et al., 2019; Draper et al., 2012; Kolassa et al., 2017; Renzullo et al., 2014). Our
892 experimental results also show that, compared to single-sensor soil moisture DA,
893 simultaneous assimilation of the ASCAT and SMAP soil moisture retrievals within the KIM-
894 LIS coupled system has a synergistic impact, improving the analyses and forecasts of
895 atmospheric variables including specific humidity, air temperature, and precipitation.

896 However, the superiority of individual single-sensor soil moisture retrieval products and their
897 combined performance within the DA system depend on the region and time period (Figure
898 6). Specifically, locally reduced benefits of SMAP or ASCAT are observed in the multi-
899 sensor soil moisture DA experiment when their performance impacts are opposite (Figure 6).
900 This may be attributed to the use of uniform observation error standard deviations for the soil
901 moisture retrievals across space and time, which is unrealistic and does not adequately reflect
902 the actual and relative retrieval skill of each soil moisture product. Especially, underestimated
903 soil moisture observation errors can degrade the soil moisture and atmospheric analyses by
904 over-relying on less reliable soil moisture data within the DA framework.

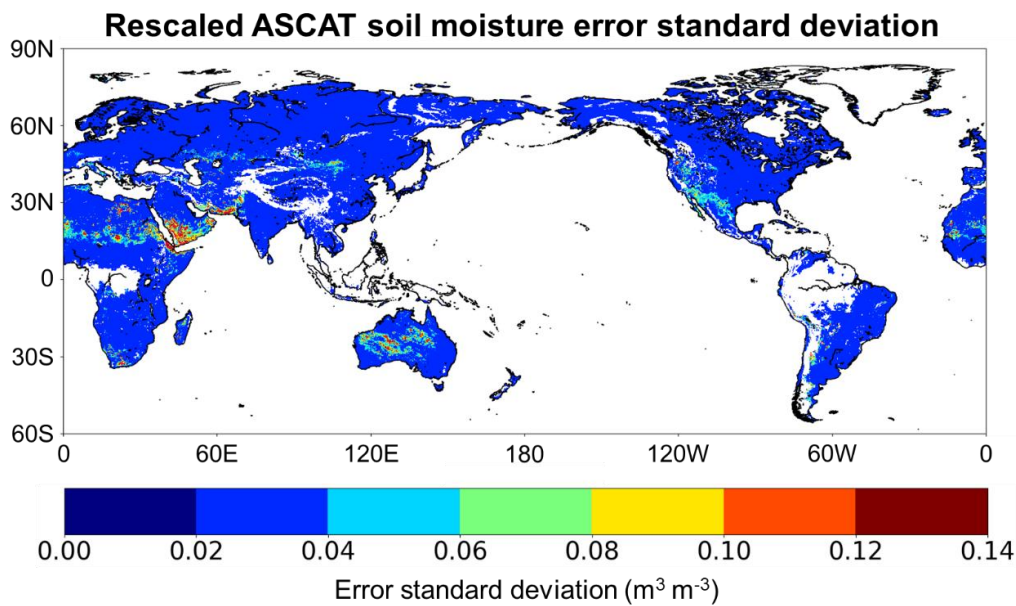
905 One key advantage of simultaneously assimilating individual soil moisture products,
906 rather than a preprocessed multi-sensor-derived soil moisture product, is the flexibility to
907 handle individual soil moisture sensors separately within a single DA system while achieving
908 comparable performance (Kolassa et al., 2017). However, this advantage can be more
909 effectively utilized by accurately specifying the relative errors of the soil moisture retrievals
910 in space and time, enabling the optimal combination of models and diverse soil moisture
911 products.

912 Several recent studies (e.g., Wu et al., 2021; Kim et al., 2023; Kim et al., 2025) have
913 made efforts to estimate spatially or spatiotemporally distributed errors in satellite-based soil
914 moisture retrievals using TCA-based methods and machine learning algorithms. A map of
915 spatially distributed (but time-invariant) error standard deviations from Kim et al. (2025) [see
916 Figure S6, which is Figure 5a in Kim et al. (2025)] exhibits that the SMAP soil moisture data
917 have errors greater than $0.05 \text{ m}^3 \text{ m}^{-3}$ in many areas, particularly in forests. Excluding forested

918 areas where soil moisture retrievals are masked out during quality control (see Section 3.4)
919 and thus not assimilated, the error standard deviations of SMAP soil moisture are still above
920 $0.02 \text{ m}^3 \text{ m}^{-3}$ (the uniformly applied error value in this study) in some savanna regions of
921 South America and Africa, grasslands in North America, and croplands in South Asia (Figure
922 S6) [see Figure S3c for the land-cover type map generated in this study using the MODIS-
923 IGBP global land-cover classification (Friedl et al., 2002)]. As a result, this leads to
924 degradation in the 2-m specific humidity and air temperature analysis in the regions, as noted
925 in the SMAP soil moisture DA (SG_SP) results shown in Figure 6.

926 Meanwhile, in ASCAT soil moisture DA, the spatially distributed soil moisture
927 observation error standard deviation ($\text{m}^3 \text{ m}^{-3}$) (Figure 8) is applied after locally rescaling the
928 uniformly specified 10% soil wetness index observation error using the ratio of the standard
929 deviations of modeled and observed soil moisture time series (see Section 4.2). However, the
930 spatial pattern of the ASCAT observation error standard deviations in Figure 8 does not
931 completely match that of the TCA/ML-based ASCAT fMSE computed by Kim et al. (2023)
932 (see their Figure 4f), which was derived using other satellite soil moisture data as triplet
933 components. Notably, the ASCAT errors used in the current study appear to be relatively
934 underestimated in dry areas of Africa and Asia (Figure 8), where the 2-m atmospheric
935 analyses are degraded by ASCAT soil moisture DA (SG_AT in Figure 6).

936



937
 938 **Figure 8.** ASCAT soil moisture error standard deviations used for ASCAT soil moisture data
 939 assimilation (DA) in this study. The spatially distributed ASCAT soil moisture errors ($\text{m}^3 \text{m}^{-3}$)
 940 are derived by rescaling the constant 10% soil wetness index using the ratio of the standard
 941 deviations of the Noah land surface model (LSM) and ASCAT soil moisture time series.
 942

943 The use of pre-generated spatial or spatiotemporal observation error estimates (e.g., Kim
 944 et al., 2025) can potentially maximize the benefits of each soil moisture product in multi-
 945 sensor soil moisture DA systems. One critical issue, however, is that bias correction of soil
 946 moisture observations, an essential procedure in soil moisture DA, may substantially alter
 947 their error characteristics, especially when rescaling-based methods like CDF matching are
 948 employed. To effectively apply spatially and temporally varying observation error estimates
 949 in multi-sensor soil moisture DA, a refined approach is needed to propagate error estimates
 950 from original soil moisture retrievals to bias-corrected soil moisture values.

951

952

953 **9. Conclusions**

954 This study develops and evaluates the NASA LIS-based multi-sensor soil moisture DA
955 framework as part of the Korean Integrated Model (KIM) weather prediction system. The
956 primary objective is to investigate the impact of simultaneously assimilating satellite-based
957 near-surface soil moisture retrievals from C-band active radar (ASCAT) and L-band passive
958 radiometer (SMAP) observations on the weather prediction performance of the KIM-LIS-
959 based land-atmosphere weakly coupled DA system. The ASCAT and SMAP soil moisture
960 data are assimilated individually (single-sensor DA) and jointly (multi-sensor DA) into the
961 Noah LSM within the KIM-LIS system, and their relative and combined efficiencies in
962 improving the global soil moisture analysis and atmospheric analysis/forecast skills are
963 evaluated. Soil moisture DA is conducted using the 1-dimensional EnKF, while atmospheric
964 DA is implemented using the hybrid 4DEnVar method with 4DIAU. The experiments are
965 performed in the global domain based on 6-hour cycling runs, which include analysis and
966 forecast, followed by 5-day predictions at 00 UTC and 12 UTC cycles.

967 TCA-based evaluations indicate that assimilating either ASCAT or SMAP soil moisture
968 data results in an overall positive effect on the global soil moisture analysis performance of
969 the Noah LSM, with global mean performance improvements of 4.0% and 10.5%,
970 respectively. Both single-sensor soil moisture DA cases (i.e., ASCAT and SMAP) enhance
971 the soil moisture performance across land cover types, with the greatest performance gains
972 observed in croplands. It should be noted that although this study employs the TCA method
973 as an alternative global-scale soil moisture evaluation approach, it has limitations,
974 particularly in constructing TCA triplets for the multi-sensor soil moisture DA experiment

975 without violating underlying assumptions. Therefore, we applied TCA only to the single-
976 sensor DA experiments, and the overall benefit of assimilating both sensors simultaneously
977 can only be inferred from the single-sensor results and the atmospheric evaluation. Future
978 studies should address this limitation to enable a more complete and robust assessment of the
979 impact of multi-sensor soil moisture DA by implementing instrumental variable (IV)-based
980 methods for estimating cross-correlated soil moisture errors, which require only two
981 independent soil moisture datasets (Dong et al., 2020).

982 Domain-averaged vertical profile RMSD metrics of the resulting atmospheric variables
983 show that better specific humidity and air temperature analyses in the lower atmosphere are
984 achieved with single-sensor SMAP DA and ASCAT DA, respectively. Compared to the
985 single-sensor soil moisture DA experiments, assimilating the ASCAT and SMAP soil
986 moisture retrievals together yields balanced performance enhancements, improving both
987 specific humidity and air temperature analyses. Evaluations indicate that soil moisture DA
988 within the KIM-LIS coupled system is particularly effective for the 2-m air temperature
989 analysis and forecast, especially in the multi-sensor soil moisture DA experiment. The
990 synergistic benefits of simultaneously assimilating both soil moisture products are regionally
991 dependent, yielding the greatest advantage when both soil moisture products have a positive
992 impact.

993 Our experiments demonstrate that, within a land-atmosphere coupled system, soil
994 moisture DA enhances precipitation forecast skill through land-atmosphere interaction
995 processes, particularly when multiple soil moisture products from diverse sources are jointly
996 assimilated. Specifically, multi-sensor soil moisture DA improves the prediction of

997 precipitation events, as evaluated using the ETS metric, across a range of precipitation
998 intensity thresholds.

999 This study suggests that simultaneously assimilating the ASCAT and SMAP soil moisture
1000 products within the KIM-LIS coupled system can leverage their complementary advantages,
1001 as demonstrated for the estimates of specific humidity, air temperature, and precipitation. The
1002 findings obtained in this study are promising for three main reasons. First, clear synergistic
1003 regional skill improvements from multi-sensor DA are evident, particularly in regions and
1004 periods where both single-sensor experiments show positive impacts. Second, the magnitude
1005 of atmospheric forecast skill improvements from both single- and multi-sensor soil moisture
1006 DA, relative to the control experiment (without soil moisture DA), is comparable to
1007 improvements reported in previous studies (e.g., Draper and Reichle, 2019; Lin and Pu, 2019;
1008 Muñoz-Sabater et al., 2019; Reichle et al., 2023), with multi-sensor DA yielding slightly
1009 better (though not statistically significant) performance. Achieving consistent improvements
1010 across the globe remains challenging due to factors discussed in Section 8, which can cause
1011 local skill degradations in atmospheric estimates. Finally, as emphasized above, simultaneous
1012 assimilation of ASCAT and SMAP produces a more balanced improvement across
1013 atmospheric variables than single-sensor DA. These results highlight the value of assimilating
1014 soil moisture observations from multiple sensors, even if trade-offs remain for certain
1015 variables in regions or periods where single-sensor impacts conflict.

1016 To conclude, a key aspect of this study is the joint assimilation of individual radar- and
1017 radiometer-based soil moisture products (multi-sensor DA) within a land-atmosphere coupled
1018 system to improve weather forecast skill. Compared to assimilating pre-blended soil moisture

1019 data, this approach is advantageous because (1) it accounts for the relative uncertainties of
1020 both sensors, which vary across space and time; (2) it provides a flexible framework for
1021 incorporating various combinations of soil moisture data sources within DA systems; and (3)
1022 it is more suitable for near-real time operational forecast systems, the focus of this study,
1023 since soil moisture data blending processes may increase latency and thereby reduce data
1024 availability for operational use. However, a direct comparison of soil moisture DA
1025 performance between the two approaches (i.e., joint assimilation of multiple products and
1026 assimilation of a pre-blended product) has not been conducted in this study. It is also
1027 acknowledged that the overall domain-averaged improvements in atmospheric estimates
1028 achieved through multi-sensor soil moisture DA, relative to single-sensor DA, are limited and
1029 statistically insignificant.

1030 The following issues remain to be addressed in future studies to enhance future
1031 performance. First, the impact of subsurface scattering on the quality of the ASCAT soil
1032 moisture product under dry soil conditions needs to be considered in quality control
1033 procedures. Second, an alternative soil moisture bias correction method, especially for
1034 ASCAT data, should be explored. Third, more realistic spatially or spatiotemporally
1035 distributed estimates of soil moisture observation errors are required to maximize the benefits
1036 of multi-sensor soil moisture DA. Lastly, as discussed in several previous studies, addressing
1037 biases in the soil moisture-latent heat flux coupling in LSMs (Crow et al., 2023; Kwon et al.,
1038 2024; Lei et al. 2018), accounting for the background error covariance between atmospheric
1039 and land variables during DA (Kwon et al., 2024), and assimilating screen-level observations

1040 (de Rosnay et al., 2013; Lin and Pu, 2020) can improve the positive impacts of soil moisture
 1041 DA on atmospheric forecast in coupled systems.

1042

1043 **Appendix A: Abbreviations**

AMSR2	Advanced Microwave Scanning Radiometer 2
AMSU-A	Advanced Microwave Sounding Unit-A
AMVs	Atmospheric Motion Vectors
ASCAT	Advanced SCATterometer
ATMS	Advanced Technology Microwave Sounder
CDF	Cumulative distribution function
CDR	Climate Data Record
CPC	Climate Prediction Center
CrIS	Cross-track Infrared Sounder
CTL	Control case serving as a baseline experiment
DA	Data assimilation
DCA	Dual Channel Algorithm
EASE	Equal Area Scalable Earth
ECMWF	European Centre for Medium-Range Weather Forecasts
EnKF	Ensemble Kalman filter
ERA5	Fifth generation of the ECMWF atmospheric reanalysis
ESA CCI	European Space Agency Climate Change Initiative
ESME	Estimated Soil Moisture Error
ETS	Equitable threat score
EUMETSAT	European Organisation for the Exploitation of Meteorological Satellites
FAO	Food and Agriculture Organization
FB	Frequency bias
fMSE	Fractional mean-square error
GLDAS	Global Land Data Assimilation System
GPS-RO	Global Positioning System Radio Occultation
Hybrid 4DEnVar	Hybrid four-dimensional ensemble variational
IASI	Infrared Atmosphere Sounding Interferometer
IFS	Integrated Forecasting System
IGBP	International Geosphere-Biosphere Programme
KIAPS	Korea Institute of Atmospheric Prediction Systems
KIM	Korean Integrated Model
KPOP	KIM Package of Observation Processing
KVAR	KIM VARiational data assimilation

LETKF	Local ensemble transform Kalman filter
LIS	Land Information System
LPRM	Land Parameter Retrieval Model
LSM	Land surface model
LST	Local solar time
L2	Level 2
MetOp	Meteorological Operational
MHS	Microwave Humidity Sounder
MODIS	Moderate resolution imaging spectroradiometer
MT_ATSP	Multi-sensor soil moisture data assimilation experiment
NASA	National Aeronautics and Space Administration
NCEP	National Centers for Environmental Prediction
NOAA	National Oceanic and Atmospheric Administration
NSIDC	National Snow and Ice Data Center
NWP	Numerical weather prediction
RFI	Radio Frequency Interference
RMSD	Root mean square difference
SG_AT	Single-sensor data assimilation experiment using the ASCAT soil moisture data
SG_SP	Single-sensor data assimilation experiment using the SMAP soil moisture data
SMAP	Soil Moisture Active Passive
SMOS	Soil Moisture and Ocean Salinity
SMOS-IC	SMOS-INRA-CESBIO
SRTM	Shuttle Radar Topography Mission
STATSGO	State Soil Geographic
TCA	Triple collocation analysis
TU Wien	Vienna University of Technology
UTC	Coordinated Universal Time
VV	Vertical transmit vertical receive
WMO	World Meteorological Organization
4DIAU	Four-dimensional incremental analysis update

1044

1045 **Code and data availability**

1046 The NASA Land Information System (LIS) framework is publicly available at

1047 <https://github.com/NASA-LIS/LISF>. Satellite-based soil moisture data assimilated in this

1048 study, i.e., Soil Moisture Active Passive (SMAP) and Advanced SCATterometer (ASCAT),

1049 can be obtained from <https://n5eil01u.ecs.nsidc.org/SMAP/SPL2SMP.009/> and

1050 <https://eoportal.eumetsat.int>, respectively. Other global soil moisture products, used as TCA
1051 triplet components to evaluate soil moisture estimates, can be downloaded from
1052 <https://www.earthdata.nasa.gov/sensors/amr2> for the Advanced Microwave Scanning
1053 Radiometer 2 (AMSR2) and [https://ib.remote-sensing.inrae.fr/index.php/smos-ic-v2-product-](https://ib.remote-sensing.inrae.fr/index.php/smos-ic-v2-product-documentation)
1054 [documentation](https://ib.remote-sensing.inrae.fr/index.php/smos-ic-v2-product-documentation) for the Soil Moisture and Ocean Salinity (SMOS) mission. Integrated
1055 Forecasting System (IFS) analysis data can be obtained from the European Centre for
1056 Medium-Range Weather Forecasts (ECMWF) in accordance with their data policy. The
1057 National Oceanic and Atmospheric Administration (NOAA) Climate Prediction Center (CPC)
1058 gauge-based global daily precipitation data can be downloaded from
1059 <https://psl.noaa.gov/data/gridded/data.cpc.globalprecip.html>. The Korean Integrated Model
1060 (KIM) software is not yet publicly available and cannot be distributed due to the Korean
1061 government's security policy. All experimental data generated in this work will be available
1062 from the authors upon request.

1063

1064 **Author contribution**

1065 YK: conceptualization, methodology, investigation, formal analysis, writing (original draft),
1066 writing (review and editing). SJ: data curation, methodology, writing (review and editing).
1067 HK: data curation, methodology, validation, writing (review and editing). KHS: validation,
1068 writing (review and editing). IHK: supervision, methodology, writing (review and editing).
1069 EK: validation, writing (review and editing). SC: validation, writing (review and editing)

1070

1071

1072 **Competing interests**

1073 The contact author has declared that none of the authors has any competing interests.

1074

1075 **Acknowledgments**

1076 This work was mainly supported by the Korea Meteorological Administration R&D project

1077 "Development of a Next-Generation Data Assimilation System by the Korea Institute of

1078 Atmospheric Prediction Systems (KIAPS)" (KMA2020-02211). Hyunglok Kim was

1079 supported by grants from the National Research Foundation of Korea (NRF), funded by the

1080 Korean government (MSIT) (RS-2025-24535700; RS-2025-02363044). We sincerely thank

1081 the scientists of the NASA LIS team for their considerable efforts in developing the LIS

1082 framework and making it publicly available. We would also like to express our gratitude to

1083 the research teams of ECMWF, ASCAT, SMAP, AMSR2, SMOS, and NOAA CPC for

1084 sharing the data used in this study.

1085

1086 **References**

1087

1088 Al-Yaari, A., Wigneron, J.-P., Dorigo, W., Colliander, A., Pellarin, T., Hahn, S., Mialon, A.,
1089 Richaume, P., Fernandez-Moran, R., Fan, L., Kerr, Y.H., De Lannoy, G., 2019.

1090 Assessment and inter-comparison of recently developed/reprocessed microwave
1091 satellite soil moisture products using ISMN ground-based measurements. *Remote Sens.*
1092 *Environ.* 224, 289–303. <https://doi.org/10.1016/j.rse.2019.02.008>.

1093 Assouline, S., 2013. Infiltration into soils: conceptual approaches and solutions. *Water*
1094 *Resour. Res.* 49, 1755–1772. <http://dx.doi.org/10.1002/wrcr.20155>.

1095 Azimi, S., Dariane, A.B., Modanesi, S., Bauer-Marschallinger, B., Bindlish, R., Wagner, W.,
1096 Massari, C., 2020. Assimilation of Sentinel 1 and SMAP – based satellite soil moisture
1097 retrievals into SWAT hydrological model: the impact of satellite revisit time and
1098 product spatial resolution on flood simulations in small basins. *J. Hydrol.* 581, 124367.
1099 <https://doi.org/10.1016/j.jhydrol.2019.124367>.

- 1100 Bartalis, Z., Wagner, W., Naeimi, V., Hasenauer, S., Scipal, K., Bonekamp, H., Figa, J.,
1101 Anderson, C., 2007. Initial soil moisture retrievals from the METOP-A Advanced
1102 Scatterometer (ASCAT). *Geophys. Res. Lett.* 34, L20401.
1103 <https://doi.org/10.1029/2007GL031088>.
- 1104 Baugh, C., de Rosnay, P., Lawrence, H., Jurlina, T., Drusch, M., Zsoter, E., Prudhomme, C.,
1105 2020. The impact of SMOS soil moisture data assimilation within the operational
1106 Global Flood Awareness System (GloFAS). *Remote Sens.* 12, 1490.
1107 <https://doi.org/10.3390/rs12091490>.
- 1108 Beljaars, A.C.M., Viterbo, P., Miller, M.J., Betts, A. K., 1996. The anomalous rainfall over
1109 the United States during July1993: Sensitivity to land surface parameterization and soil
1110 moisture anomalies. *Mon. Weather Rev.* 124, 362–383. [https://doi.org/10.1175/1520-0493\(1996\)124<0362:TAROTU>2.0.CO;2](https://doi.org/10.1175/1520-0493(1996)124<0362:TAROTU>2.0.CO;2).
- 1112 Ben Bouallègue, Z., Clare, M.C.A., Magnusson, L., Gascón, E., Maier-Gerber, M., Janoušek,
1113 M., Rodwell, M., Pinault, F., Dramsch, J.S., Lang, S.T.K., Raoult, B., Rabier, F.,
1114 Chevallier, M., Sandu, I., Dueben, P., Chantry, M., Pappenberger, F., 2024. A first
1115 statistical assessment of machine learning-based weather forecasts in an operational-
1116 like context. *B. Am. Meteorol. Soc.* 105, E864–E883. <https://doi.org/10.1175/BAMS-D-23-0162.1>.
- 1118 Bhuiyan, H., McNairn, H., Powers, J., Friesen, M., Pacheco, A., Jackson, T. J., Cosh, M. H.,
1119 Colliander, A., Berg, A., Rowlandson, T., Bullock, P., Magagi, R., 2018. Assessing
1120 SMAP soil moisture scaling and retrieval in the carman (Canada) study site. *Vadose
1121 Zone J.* 17, 180132. <https://doi.org/10.2136/vzj2018.07.0132>.
- 1122 Blyverket, J., Hamer, P.D., Bertino, L., Albergel, C., Fairbairn, D., Lahoz, W.A., 2019. An
1123 evaluation of the EnKF vs. EnOI and the assimilation of SMAP, SMOS and ESA CCI
1124 soil moisture data over the contiguous US. *Remote Sens.* 11, 478.
1125 <https://doi.org/10.3390/rs11050478>.
- 1126 Bolten, J.D., Crow, W.T., Zhan, X., Jackson, T.J., Reynolds, C.A., 2010. Evaluating the
1127 utility of remotely sensed soil moisture retrievals for operational agricultural drought
1128 monitoring, *IEEE J. Sel. Top. Appl. Earth Obs. Remote Sens.* 3, 57–66.
1129 <https://doi.org/10.1109/JSTARS.2009.2037163>.
- 1130 Bosilovich, M.G., Sun, W.-Y., 1999 Numerical simulation of the 1993 Midwestern flood:
1131 Land–atmosphere interactions. *J. Climate* 12, 1490–1505.
1132 [https://doi.org/10.1175/1520-0442\(1999\)012<1490:NSOTMF>2.0.CO;2](https://doi.org/10.1175/1520-0442(1999)012<1490:NSOTMF>2.0.CO;2).
- 1133 Brocca, L., Melone, F., Moramarco, T., Wagner, W., Naeimi, V., Bartalis, Z., Hasenauer, S.,
1134 2010. Improving runoff prediction through the assimilation of the ASCAT soil
1135 moisture product. *Hydrol. Earth Syst. Sci.* 14, 1881–1893.
1136 <http://dx.doi.org/10.5194/hess-14-1881-2010>.
- 1137 Catalano, F., Alessandri, A., De Felice, M., Zhu, Z., Myneni, R.B., 2016. Observationally
1138 based analysis of land–atmosphere coupling. *Earth Syst. Dynam.* 7, 251–266.
1139 <https://doi.org/10.5194/esd-7-251-2016>.
- 1140 Chan, S.K., Bindlish, R., O’Neill, P., Jackson, T., Njoku, E., Dunbar, S., Chaubell, J.,
1141 Piepmeier, J., Yueh, S., Entekhabi, D., Colliander, A., Chen, F., Cosh, M.H., Caldwell,
1142 T., Walker, J., Berg, A., McNairn, H., Thibeault, M., Martínez-Fernández, J., Uldall, F.,

1143 Seyfried, M., Bosch, D., Starks, P., Holifield Collins, C., Prueger, J., van der Velde, R.,
 1144 Asanuma, J., Palecki, M., Small, E.E., Zreda, M., Calvet, J., Crow, W.T., Kerr, Y.,
 1145 2018. Development and assessment of the SMAP enhanced passive soil moisture
 1146 product. *Remote Sens. Environ.* 204, 931–941.
 1147 <https://doi.org/10.1016/j.rse.2017.08.025>.
 1148 Chaubell, M.J., Yueh, S.H., Dunbar, R.S., Colliander, A., Chen, F., Chan, S.K., Entekhabi, D.,
 1149 Bindlish, R., O’Neill, P.E., Asanuma, J., Berg, A.A., Bosch, D.D., Caldwell, T., Cosh,
 1150 M.H., Collins, C.H., Martínez-Fernández, J., Seyfried, M., Starks, P.J., Su, Z.,
 1151 Thibeault, M., Walker, J., 2020. Improved SMAP dual-channel algorithm for the
 1152 retrieval of soil moisture. *IEEE Trans. Geosci. Remote Sens.* 58, 3894–3905.
 1153 <https://doi.org/10.1109/tgrs.2019.2959239>.
 1154 Chen, M., Shi, W., Xie, P., Silva, V.B.S., Kousky, V.E., Higgins, R.W., Janowiak, J.E., 2008.
 1155 Assessing objective techniques for gauge-based analyses of global daily precipitation. *J.*
 1156 *Geophys. Res.* 113, D04110. <https://doi.org/10.1029/2007JD009132>.
 1157 Cho, E., Kwon, Y., Kumar, S.V., Vuyovich, C.M., 2023. Assimilation of airborne gamma
 1158 observations provides utility for snow estimation in forested environments. *Hydrol.*
 1159 *Earth Syst. Sci.* 27, 4039–4056. <https://doi.org/10.5194/hess-27-4039-2023>.
 1160 Colliander, A., Jackson, T.J., Bindlish, R., Chan, S., Das, N., Kim, S. B. et al., 2017.
 1161 Validation of SMAP surface soil moisture products with core validation sites. *Remote*
 1162 *Sens. Environ.* 191, 215–231. <https://doi.org/10.1016/j.rse.2017.01.021>.
 1163 Cook, B.I., Bonan, G.B., Levis, S., 2006. Soil moisture feedbacks to precipitation in southern
 1164 Africa. *J. Climate* 19, 4198–4206. <https://doi.org/10.1175/JCLI3856.1>.
 1165 Crow, W.T., Van den Berg, M.J., 2010. An improved approach for estimating observation
 1166 and model error parameters in soil moisture data assimilation. *Water Resour. Res.* 46,
 1167 W12519. <https://doi.org/10.1029/2010WR009402>.
 1168 Crow, W.T., Kim, H., Kumar, S., 2023. Systematic modelling errors undermine the
 1169 application of land data assimilation systems for hydrological and weather forecasting.
 1170 *J. Hydrometeor.* 25, 3–26. <https://doi.org/10.1175/JHM-D-23-0069.1>.
 1171 Dare, R.A., Ebert, E.E., 2017. Latitudinal variations in the accuracy of model-generated
 1172 forecasts of precipitation over Australia and south-east Asia. *J. South. Hemisph. Earth*
 1173 *Syst. Sci.* 67, 46–63. <https://doi.org/10.1071/ES17005>.
 1174 Das, N.N., Entekhabi, D., Dunbar, R.S., Chaubell, M.J., Colliander, A., Yueh, S., Jagdhuber,
 1175 T., Chen, F., Crow, W., O’Neill, P.E., Walker, J.P., Berg, A., Bosch, D.D., Caldwell,
 1176 T., Cosh, M.H., Collins, C.H., Lopez-Baeza, E., Thibeault, M., 2019. The SMAP and
 1177 Copernicus Sentinel-1A/B microwave active passive high resolution surface soil
 1178 moisture product. *Remote Sens. Environ.* 233, 111380.
 1179 <https://doi.org/10.1016/j.rse.2019.111380>.
 1180 Dee, D.P., Da Silva, A.M., 1998. Data assimilation in the presence of forecast bias. *Quart. J.*
 1181 *Roy. Meteor. Soc.* 124, 269–295. <https://doi.org/10.1002/qj.49712454512>.
 1182 de Rosnay, P., Drusch, M., Vasiljevic, D., Balsamo, G., Albergel, C., Isaksen, L., 2013. A
 1183 simplified extended Kalman filter for the global operational soil moisture analysis at
 1184 ECMWF. *Q. J. Roy. Meteor. Soc.* 139, 1199–1213. <https://doi.org/10.1002/qj.2023>.

1185 de Rosnay, P., Browne, P., de Boissésou, E., Fairbairn, D., Hirahara, Y. et al., 2022. Coupled
1186 data assimilation at ECMWF: current status, challenges and future developments. *Q. J.*
1187 *Roy. Meteor. Soc.* 148, 2672–2702. <https://doi.org/10.1002/qj.4330>.

1188 Dirmeyer, P., Halder, S., 2016. Sensitivity of numerical weather forecasts to initial soil
1189 moisture variations in CFSv2. *Wea. Forecasting* 31, 1973–1983.
1190 <https://doi.org/10.1175/WAF-D-16-0049.1>.

1191 Dobson, M.C., Ulaby, F.T., 1986. Active microwave soil moisture research. *IEEE Trans.*
1192 *Geosci. Remote Sens.* GE-24, 23–36. <https://doi.org/10.1109/TGRS.1986.289585>.

1193 Dong, J., Wei, L., Chen, X., Duan, Z., Lu, Y., 2020. An instrument variable based algorithm
1194 for estimating cross-correlated hydrological remote sensing errors. *J. Hydrol.* 581,
1195 124413. <https://doi.org/10.1016/j.jhydrol.2019.124413>.

1196 Dorigo, W.A., Scipal, K., Parinussa, R.M., Liu, Y.Y., Wagner, W., De Jeu, R.A.M., Naeimi,
1197 V., 2010. Error characterisation of global active and passive microwave soil moisture
1198 datasets. *Hydrol. Earth Syst. Sci.* 14, 2605–2616. [https://doi.org/10.5194/hess-14-2605-](https://doi.org/10.5194/hess-14-2605-2010)
1199 2010.

1200 Dorigo, W., Wagner, W., Albergel, C., Albrecht, F., Balsamo, G., Brocca, L., Chung, D., Ertl,
1201 M., Forkel, M., Gruber, A., Haas, E., Hamer, P.D., Hirschi, M., Ikonen, J., de Jeu, R.,
1202 Kidd, R., Lahoz, W., Liu, Y.Y., Miralles, D., Mistelbauer, T., Nicolai-Shaw, N.,
1203 Parinussa, R., Pratola, C., Reimer, C., van der Schalie, R., Seneviratne, S.I., Smolander,
1204 T., Lecomte, P., 2017. ESA CCI soil moisture for improved Earth system
1205 understanding: state-of-the art and future directions. *Remote Sens. Environ.* 203, 185–
1206 215. <https://doi.org/10.1016/j.rse.2017.07.001>.

1207 Draper, C.S., Mahfouf, J.-F., Walker, J.P., 2011. Root-zone soil moisture from the
1208 assimilation of screen-level variables and remotely sensed soil moisture. *J. Geophys.*
1209 *Res.* 116, D02127. <https://doi.org/10.1029/2010JD013829>.

1210 Draper, C.S., Reichle, R.H., De Lannoy, G.J.M., Liu, Q., 2012. Assimilation of passive and
1211 active microwave soil moisture retrievals. *Geophys. Res. Lett.* 39, L04401.
1212 <https://doi.org/10.1029/2011GL050655>.

1213 Draper, C., Reichle, R., de Jeu, R., Naeimi, V., Parinussa, R., Wagner, W., 2013. Estimating
1214 root mean square errors in remotely sensed soil moisture over continental scale
1215 domains. *Remote Sens. Environ.* 137, 288–298.
1216 <https://doi.org/10.1016/j.rse.2013.06.013>.

1217 Draper, C., Reichle, R.H., 2019. Assimilation of satellite soil moisture for improved
1218 atmospheric reanalyses. *Mon. Weather Rev.* 147, 2163–2188.
1219 <https://doi.org/10.1175/MWR-D-18-0393.1>.

1220 Drusch, M., Viterbo, P., 2007. Assimilation of screen-level variables in ECMWF's Integrated
1221 Forecast System: A study on the impact on the forecast quality and analyzed soil
1222 moisture. *Mon. Weather Rev.* 135, 300–314. <https://doi.org/10.1175/MWR3309.1>.

1223 ECMWF, 2017. IFS Documentation CY43R3 - Part II: Data assimilation. European Centre
1224 for Medium-Range Weather Forecasts, Reading, UK, 103 pp.
1225 <https://doi.org/10.21957/v61kmv92i>.

1226 Ek, M.B., Mitchell, K.E., Lin, Y., Rogers, E., Grunmann, P., Koren, V., Gayno, G., Tarpley,
1227 J.D., 2003. Implementation of Noah land surface model advances in the National

1228 Centers for Environmental Prediction operational mesoscale Eta model. *J. Geophys.*
1229 *Res.* 108, 8851. <https://doi.org/10.1029/2002JD003296>.

1230 Entekhabi, D., Njoku, E.G., O'Neill, P.E., Kellogg, K.H., Crow, W.T., Edelstein, W.N., 2010.
1231 The soil moisture active passive (SMAP) mission. *Proc. IEEE* 98, 704–716.
1232 <https://doi.org/10.1109/JPROC.2010.2043918>.

1233 Evensen, G., 1994. Sequential data assimilation with a nonlinear quasi-geostrophic model
1234 using Monte Carlo methods to forecast error statistics. *J. Geophys. Res.* 99, 10143–
1235 10162. <https://doi.org/10.1029/94JC00572>.

1236 Fairbairn, D., de Rosnay, P., Weston, P., 2024. Evaluation of an adaptive soil moisture bias
1237 correction approach in the ECMWF land data assimilation system. *Remote Sens.* 16,
1238 493. <https://doi.org/10.3390/rs16030493>.

1239 Farr, T.G., Rosen, P.A., Caro, E., Crippen, R., Duren, R., Hensley, S., Kobrick, M., Paller, M.,
1240 Rodriguez, E., Roth, L., Seal, D., Shaffer, S., Shimada, J., Umland, J., Werner, M.,
1241 Oskin, M., Burbank, D., Alsdorf, D., 2007. The shuttle radar topography mission. *Rev.*
1242 *Geophys.* 45, RG2004. <https://doi.org/10.1029/2005RG000183>.

1243 Ferguson, C.R., Agrawal, S., Beauharnois, M.C., Xia, G., Burrows, D.A., Bosart, L.F., 2020.
1244 Assimilation of satellite-derived soil moisture for improved forecasts of the great plains
1245 low-level jet. *Mon. Weather Rev.* 148, 4607–4627. <https://doi.org/10.1175/MWR-D-20-0185.1>.

1247 Findell, K.L., Eltahir, E.A.B., 2003. Atmospheric controls on soil moisture–boundary layer
1248 interactions. Part I: Framework development. *J. Hydrometeor.* 4, 552–569.
1249 [https://doi.org/10.1175/1525-7541\(2003\)004<0552:ACOSML>2.0.CO;2](https://doi.org/10.1175/1525-7541(2003)004<0552:ACOSML>2.0.CO;2).

1250 Friedl, M.A., McIver, D.K., Hodges, J.C.F., Zhang, X.Y., Muchoney, D., Strahler, A.H.,
1251 Woodcock, C.E., Gopal, S., Schneider, A., Cooper, A., Baccini, A., Gao, F., Schaaf, C.,
1252 2002. Global land cover mapping from MODIS: algorithms and early results. *Remote*
1253 *Sens. Environ.* 83, 287–302. [https://doi.org/10.1016/S0034-4257\(02\)00078-0](https://doi.org/10.1016/S0034-4257(02)00078-0).

1254 Fuentes, I., Padarian, J., Vervoort, R.W., 2022. Towards near real-time national-scale soil
1255 water content monitoring using data fusion as a downscaling alternative. *J. Hydrol.* 609,
1256 127705. <https://doi.org/10.1016/j.jhydrol.2022.127705>.

1257 Gavahi, K., Abbaszadeh, P., Moradkhani, H., 2022. How does precipitation data influence the
1258 land surface data assimilation for drought monitoring? *Sci. Total Environ.* 831, 154916.
1259 <https://doi.org/10.1016/j.scitotenv.2022.154916>.

1260 Gentine, P., Polcher, J., Entekhabi, D., 2011. Harmonic propagation of variability in surface
1261 energy balance within a coupled soil–vegetation–atmosphere system. *Water Resour.*
1262 *Res.* 47, W05525. <http://dx.doi.org/10.1029/2010WR009268>.

1263 Gruber, A., Su, C.-H., Zwieback, S., Crow, W., Dorigo, W., Wagner, W., 2016. Recent
1264 advances in (soil moisture) triple collocation analysis. *Int. J. Appl. Earth Obs.* 45, 200–
1265 211. <https://doi.org/10.1016/j.jag.2015.09.002>.

1266 Hersbach, H., Bell, B., Berrisford, P., Hirahara, S., Horányi, A., Muñoz-Sabater, J., Nicolas,
1267 J., Peubey, C., Radu, R., Schepers, D., et al., 2020. The ERA5 global reanalysis. *Q. J.*
1268 *Roy. Meteorol. Soc.* 146, 1999–2049. <https://doi.org/10.1002/qj.3803>.

- 1269 Hohenegger, C., Brockhaus, P., Bretherton, C.S., Schär, C., 2009. The soil moisture–
1270 precipitation feedback in simulations with explicit and parameterized convection. *J.*
1271 *Climate* 22, 5003–5020. <https://doi.org/10.1175/2009JCLI2604.1>.
- 1272 Hong, S.-Y., Kwon, Y.C., Kim, T.-H., Kim, J.-E.E., Choi, S.-J., Kwon, I.-H., Kim, J., Lee,
1273 E.-H., Park, R.-S., and Kim, D.-I., 2018. The Korean Integrated Model (KIM) system
1274 for global weather forecasting. *Asia-Pac. J. Atmos. Sci.* 54, 267–292.
1275 <https://doi.org/10.1007/s13143-018-0028-9>.
- 1276 Huang, S., Zhang, X., Wang, C., Chen, N., 2023. Two-step fusion method for generating 1
1277 km seamless multi-layer soil moisture with high accuracy in the Qinghai-Tibet plateau.
1278 *ISPRS J. Photogramm.* 197, 346–363. <https://doi.org/10.1016/j.isprsjprs.2023.02.009>.
- 1279 Huang, S., Zhang, X., Chen, N., Ma, H., Fu, P., Dong, J., Gu, X., Nam, W.-H., Xu, L., Rab,
1280 G., Niyogi, D., 2022. A novel fusion method for generating surface soil moisture data
1281 with high accuracy, high spatial resolution, and high spatiotemporal continuity. *Water*
1282 *Resour. Res.* 58, e2021WR030827. <https://doi.org/10.1029/2021WR030827>.
- 1283 Jalilvand, E., Tajrishy, M., Hashemi, S.A.G.Z., Brocca, L., 2019. Quantification of irrigation
1284 water using remote sensing of soil moisture in a semi-arid region. *Remote Sens.*
1285 *Environ.* 231, 111226. <https://doi.org/10.1016/j.rse.2019.111226>.
- 1286 Jiang, M., Qiu, T., Wang, T., Zeng, C., Zhang, B., Shen, H., 2025. Seamless global daily soil
1287 moisture mapping using deep learning based spatiotemporal fusion. *Int. J. Appl. Earth*
1288 *Obs.* 139, 104517. <https://doi.org/10.1016/j.jag.2025.104517>.
- 1289 Jun, S., Park, J.-H., Choi, H.-J., Lee, Y.-H., Lim, Y.-J., Boo, K.-O., Kang, H.-S., 2021.
1290 Impact of soil moisture data assimilation on analysis and medium-range forecasts in an
1291 operational global data assimilation and prediction system. *Atmosphere* 12, 1089.
1292 <https://doi.org/10.3390/atmos12091089>.
- 1293 Kang, J.-H., Chun, H.-W., Lee, S., Ha, J.-H., Song, H.-J., Kwon, I.-H., Han, H.-J., Jeong, H.,
1294 Kwon, H.-N., Kim, T.-H., 2019. Development of an observation processing package
1295 for data assimilation in KIAPS. *Asia-Pac. J. Atmos. Sci.* 54, 303–318.
1296 <https://doi.org/10.1007/s13143-018-0030-2>.
- 1297 Keppenne, C.L., 2000. Data assimilation into a primitive-equation model with a parallel
1298 ensemble Kalman filter. *Mon. Weather Rev.* 128, 1971–1981.
1299 [https://doi.org/10.1175/1520-0493\(2000\)128<1971:DAIAPE>2.0.CO;2](https://doi.org/10.1175/1520-0493(2000)128<1971:DAIAPE>2.0.CO;2).
- 1300 Kerr, Y.H., Waldteufel, P., Richaume, P., Wigneron, J.P., Ferrazzoli, P., Mahmoodi, A., Al
1301 Bitar, A., Cabot, F., Gruhier, C., Juglea, S.E., Leroux, D., Mialon, A., Delwart, S.,
1302 2012. The SMOS soil moisture retrieval algorithm. *IEEE Trans. Geosci. Remote Sens.*
1303 50, 1384–1403. <https://doi.org/10.1109/TGRS.2012.2184548>.
- 1304 Khaki, M., Awange, J., 2019. The application of multi-mission satellite data assimilation for
1305 studying water storage changes over South America. *Sci. Total Environ.* 647, 1557–
1306 1572. <https://doi.org/10.1016/j.scitotenv.2018.08.079>.
- 1307 Khaki, M., Hendricks Franssen, H.-J., Han, S.C., 2020. Multi-mission satellite remote
1308 sensing data for improving land hydrological models via data assimilation. *Sci. Rep.* 10,
1309 18791. <https://doi.org/10.1038/s41598-020-75710-5>.

1310 Khaki, M., Hoteit, I., Kuhn, M., Forootan, E., Awange, J., 2019. Assessing data assimilation
1311 frameworks for using multi-mission satellite products in a hydrological context. *Sci.*
1312 *Total Environ.* 647, 1031–1043. <https://doi.org/10.1016/j.scitotenv.2018.08.032>.

1313 Kim, H., Parinussa, R., Konings, A.G., Wagner, W., Cosh, M.H., Lakshmi, V., Zohaib, M.,
1314 Choi, M., 2018. Global-scale assessment and combination of SMAP with ASCAT
1315 (active) and AMSR2 (passive) soil moisture products. *Remote Sens. Environ.* 204,
1316 260–275. <https://doi.org/10.1016/j.rse.2017.10.026>.

1317 Kim, H., Wigneron, J.-P., Kumar, S., Dong, J., Wagner, W., Cosh, M.H., Bosch, D.D.,
1318 Collins, C.H., Starks, P.J., Seyfried, M., Lakshmi, V., 2020. Global scale error
1319 assessments of soil moisture estimates from microwave-based active and passive
1320 satellites and land surface models over forest and mixed irrigated/dryland agriculture
1321 regions. *Remote Sens. Environ.* 251, 112052. <https://doi.org/10.1016/j.rse.2020.112052>.

1322 Kim, H., Lakshmi, V., Kwon, Y., Kumar, S.V., 2021a. First attempt of global-scale
1323 assimilation of subdaily scale soil moisture estimates from CYGNSS and SMAP into a
1324 land surface model. *Environ. Res. Lett.* 16, 074041. [https://doi.org/10.1088/1748-](https://doi.org/10.1088/1748-9326/ac0ddf)
1325 [9326/ac0ddf](https://doi.org/10.1088/1748-9326/ac0ddf).

1326 Kim, H., Lee, S., Cosh, M.H., Lakshmi, V., Kwon, Y., McCarty, G.W., 2021b. Assessment
1327 and combination of SMAP and Sentinel-1A/B-derived soil moisture estimates with
1328 land surface model outputs in the Mid-Atlantic Coastal Plain, USA. *IEEE Trans. Geosci.*
1329 *Remote Sens.* 59, 991–1011. <https://doi.org/10.1109/TGRS.2020.2991665>.

1330 Kim, H., Crow, W., Li, X., Wagner, W., Hahn, S., Lakshmi, V., 2023. True global error maps
1331 for SMAP, SMOS, and ASCAT soil moisture data based on machine learning and
1332 triple collocation analysis. *Remote Sens. Environ.* 298, 113776.
1333 <https://doi.org/10.1016/j.rse.2023.113776>.

1334 Kim, S., Kim, H., Kwon, Y., Nguyen, H.H., 2025. A stand-alone framework for predicting
1335 spatiotemporal errors in satellite-based soil moisture using tree-based models and deep
1336 neural networks. *Gisci. Remote Sens.* (minor revision).

1337 Kolassa, J., Reichle, R.H., Draper, C.S., 2017. Merging active and passive microwave
1338 observations in soil moisture data assimilation. *Remote Sens. Environ.* 191, 117–130.
1339 <https://doi.org/10.1016/j.rse.2017.01.015>.

1340 Koo, M.-S., Baek, S., Seol, K.-H., Cho, K., 2017. Advances in land modeling of KIAPS
1341 based on the Noah land surface model. *Asia-Pac. J. Atmos. Sci.* 53, 361–373.
1342 <https://doi.org/10.1007/s13143-017-0043-2>.

1343 Koster, R.D., Dirmeyer, P.A., Guo, Z., Bonan, G., Chan, E., Cox, P., Gordon, C.T., Kanae, S.,
1344 Kowalczyk, E., Lawrence, D., Liu, P., Lu, C.-H., Malyshev, S., Mcavaney, B., Mitchell,
1345 K., Mocko, D., Oki, T., Oleson, K., Pitman, A., Sud, Y.C., Taylor, C.M., Verseghy, D.,
1346 Vasic, R., Xue, Y., Yamada, T., 2004. Regions of strong coupling between soil
1347 moisture and precipitation. *Science* 305, 1138–1140.
1348 <https://doi.org/10.1126/science.1100217>.

1349 Koster, R.D., Guo, Z., Yang, R., Dirmeyer, P.A., Mitchell, K., Puma, M.J., 2009. On the
1350 nature of soil moisture in land surface models. *J. Clim.* 22, 4322–4335.
1351 <https://doi.org/10.1175/2009JCLI2832.1>.

- 1352 Koster, R.D., Mahanama, S.P.P., Yamada, T.J., Balsamo, G., Berg, A.A., Boisserie, M.,
 1353 Dirmeyer, P.A., Doblus-Reyes, F.J., Drewitt, G., Gordon, C.T., Guo, Z., Jeong, J.-H.,
 1354 Lawrence, D.M., Lee, W.-S., Li, Z., Luo, L., Malyshev, S., Merryfield, W.J.,
 1355 Seneviratne, S.I., Stanelle, T., van den Hurk, B.J.J.M., Vitart, F., Wood, E.F., 2010.
 1356 Contribution of land surface initialization to subseasonal forecast skill: first results
 1357 from a multi-model experiment. *Geophys. Res. Lett.* 37, L02402.
 1358 <https://doi.org/10.1029/2009GL041677>.
- 1359 Kumar, S.V., Peters-Lidard, C.D., Tian, Y., Houser, P.R., Geiger, J., Olden, S., Lighty, L.,
 1360 Eastman, J.L., Dotu, B., Dirmeyer, P., Adams, J., Mitchell, K., Wood, E.F., Sheffield,
 1361 J., 2006. Land information system: an interoperable framework for high resolution land
 1362 surface modeling. *Environ. Modell. Softw.* 21, 1402–1415.
 1363 <https://doi.org/10.1016/j.envsoft.2005.07.004>.
- 1364 Kumar, S.V., Reichle, R.H., Peters-Lidard, C.D., Koster, R.D., Zhan, X., Crow, W.T.,
 1365 Eylander, J.B., Houser, P.R., 2008a. A land surface data assimilation framework using
 1366 the land information system: Description and applications. *Adv. Water Resour.* 31,
 1367 1419–1432. <https://doi.org/10.1016/j.advwatres.2008.01.013>.
- 1368 Kumar, S., Peters-Lidard, C., Tian, Y., Reichle, R.H., Geiger, J., Alonge, C., Eylander, J.,
 1369 Houser, P., 2008b. An integrated hydrologic modeling and data assimilation framework.
 1370 *Computer* 41, 52–59. <https://doi.org/10.1109/MC.2008.475>.
- 1371 Kumar, S.V., Reichle, R.H., Koster, R.D., Crow, W.T., Peters-Lidard, C.D., 2009. Role of
 1372 subsurface physics in the assimilation of surface soil moisture observations. *J.*
 1373 *Hydrometeorol.* 10, 1534–1547. <https://doi.org/10.1175/2009JHM1134.1>.
- 1374 Kumar, S.V., Peters-Lidard, C.D., Mocko, D., Reichle, R., Liu, Y., Arsenault, K.R., Xia, Y.,
 1375 Ek, M., Riggs, G., Livneh, B., Cosh, M., 2014. Assimilation of remotely sensed soil
 1376 moisture and snow depth retrievals for drought estimation. *J. Hydrometeorol.* 15, 2446–
 1377 2469, <https://doi.org/10.1175/JHM-D-13-0132.1>.
- 1378 Kumar, S.V., Peters-Lidard, C.D., Santanello, J.A., Reichle, R.H., Draper, C.S., Koster, R.D.,
 1379 Nearing, G., Jasinski, M.F., 2015. Evaluating the utility of satellite soil moisture
 1380 retrievals over irrigated areas and the ability of land data assimilation methods to
 1381 correct for unmodeled processes. *Hydrol. Earth Syst. Sci.* 19, 4463–4478.
 1382 <https://doi.org/10.5194/hess-19-4463-2015>.
- 1383 Kumar, S.V., Dong, J., Peters-Lidard, C.D., Mocko, D., Gómez, B., 2017. Role of forcing
 1384 uncertainty and background model error characterization in snow data assimilation.
 1385 *Hydrol. Earth Syst. Sci.* 21, 2637–2647. <https://doi.org/10.5194/hess-21-2637-2017>.
- 1386 Kumar, S.V., Dirmeyer, P.A., Peters-Lidard, C.D., Bindlish, R., Bolten, J., 2018. Information
 1387 theoretic evaluation of satellite soil moisture retrievals. *Remote Sens. Environ.* 204,
 1388 392–400. <https://doi.org/10.1016/j.rse.2017.10.016>.
- 1389 Kumar, S.V., Jasinski, M., Mocko, D.M., Rodell, M., Borak, J., Li, B., Beaudoin, H.K.,
 1390 Peters-Lidard, C.D., 2019. NCA-LDAS land analysis: Development and performance
 1391 of a multisensory, multivariate land data assimilation system for the national climate
 1392 assessment. *J. Hydrometeorol.* 20, 1571–1593. <https://doi.org/10.1175/JHM-D-17-0125.1>.
- 1393

- 1394 Kwon, I.-H., Song, H.-J., Ha, J.-H., Chun, H.-W., Kang, J.-H., Lee, S., Lim, S., Jo, Y., Han,
1395 H.-J., Jeong, H., Kwon, H.-N., Shin, S., Kim, T.-H., 2018. Development of an
1396 operational hybrid data assimilation system at KIAPS. *Asia-Pac. J. Atmos. Sci.* 54,
1397 319–335. <https://doi.org/10.1007/s13143-018-0029-8>.
- 1398 Kwon, Y., Forman, B.A., Ahmad, J.A., Kumar, S.V., Yoon, Y., 2019. Exploring the utility of
1399 machine learning-based passive microwave brightness temperature data assimilation
1400 over terrestrial snow in High Mountain Asia. *Remote Sens.* 11, 2265.
1401 <https://doi.org/10.3390/rs11192265>.
- 1402 Kwon, Y., Yoon, Y., Forman, B.A., Kumar, S.V., Wang, L., 2021. Quantifying the
1403 observational requirements of a space-borne LiDAR snow mission. *J. Hydrol.* 601,
1404 126709. <https://doi.org/10.1016/j.jhydrol.2021.126709>.
- 1405 Kwon, Y., Kumar, S.V., Navari, M., Mocko, D.M., Kemp, E.M., Wegiel, J.W., Geiger, J.V.,
1406 Bindlish, R., 2022. Irrigation characterization improved by the direct use of SMAP soil
1407 moisture anomalies within a data assimilation system. *Environ. Res. Lett.* 17, 084006.
1408 <https://doi.org/10.1088/1748-9326/ac7f49>.
- 1409 Kwon, Y., Jun, S., Kim, E., Seol, K.-H., Hong, S., Kwon, I.-H., Kang, J.-H., Kim, H., 2024.
1410 Improving weather forecast skill of the Korean Integrated Model by assimilating Soil
1411 Moisture Active Passive soil moisture anomalies. *Q. J. Roy. Meteor. Soc.* 150, 5305–
1412 5336. <https://doi.org/10.1002/qj.4871>.
- 1413 Laiolo, P., Gabellani, S., Campo, L., Silvestro, F., Delogu, F., Rudari, R., Pulvirenti, L., Boni,
1414 G., Fascetti, F., Pierdicca, N., Crapolicchio, R., Hasenauer, S., Puca, S., 2016. Impact
1415 of different satellite soil moisture products on the predictions of a continuous
1416 distributed hydrological model. *Int. J. Appl. Earth Obs.* 48, 131–145.
1417 <https://doi.org/10.1016/j.jag.2015.06.002>.
- 1418 Lamichhane, M., Mehan, S., Mankin, K.R., 2025. Surface soil moisture prediction using
1419 multimodal remote sensing data fusion and machine learning algorithms in semi-arid
1420 agricultural region. *Sci. Remote Sens.* 12, 100255.
1421 <https://doi.org/10.1016/j.srs.2025.100255>.
- 1422 Lee, S., Song, H.-J., Chun, H.-W., Kwon, I.-H., Kang, J.-H., Lim, S., 2020. All-sky
1423 microwave humidity sounder assimilation in the Korean Integrated Model forecast
1424 system. *Q. J. Roy. Meteor. Soc.* 146, 3570-3586. <https://doi.org/10.1002/qj.3862>.
- 1425 Lei, F., Crow, W.T., Holmes, T.R.H., Hain, C., Anderson, M.C., 2018. Global investigation
1426 of soil moisture and latent heat flux coupling strength. *Water Resour. Res.* 54, 8196–
1427 8215. <https://doi.org/10.1029/2018WR023469>.
- 1428 Li, S., Zhang, L., Ma, R., Yan, M., Tian, X., 2020. Improved ET assimilation through
1429 incorporating SMAP soil moisture observations using a coupled process model: A
1430 study of U.S. arid and semiarid regions. *J. Hydrol.* 590, 125402.
1431 <https://doi.org/10.1016/j.jhydrol.2020.125402>.
- 1432 Lievens, H., De Lannoy, G.J.M., Al Bitar, A., Drusch, M., Dumedah, G., Hendricks Franssen,
1433 H.-J., Kerr, Y.H., Tomer, S.K., Martens, B., Merlin, O., Pan, M., Roundy, J.K.,
1434 Vereecken, H., Walker, J.P., Wood, E.F., Verhoest, N.E.C., Pauwels, V.R.N., 2016.
1435 Assimilation of SMOS soil moisture and brightness temperature products into a land

1436 surface model. *Remote Sens. Environ.* 180, 292–304.
1437 <https://doi.org/10.1016/j.rse.2015.10.033>.

1438 Lin, X., Huang, S., Li, J., Huang, Q., Shi, H., She, D., Leng, G., Wei, X., Guo, W., Liu, Y.,
1439 Luo, J., 2023. Feedback dynamics between precipitation, temperature, and soil
1440 moisture in China and their possible driving mechanisms under a changing
1441 environment. *Atmos. Res.* 294, 106983.
1442 <https://doi.org/10.1016/j.atmosres.2023.106983>.

1443 Lin, L.-F., Pu, Z., 2019. Examining the impact of SMAP soil moisture retrievals on short-
1444 range weather prediction under weakly and strongly coupled data assimilation with
1445 WRF-Noah. *Mon. Weather Rev.* 147, 4345–4366. <https://doi.org/10.1175/MWR-D-19-0017.1>.

1446
1447 Lin, L.-F., Pu, Z., 2020. Improving near-surface short-range weather forecasts using strongly
1448 coupled land–atmosphere data assimilation with GSI-EnKF. *Mon. Weather Rev.* 148,
1449 2863–2888. <https://doi.org/10.1175/MWR-D-19-0370.1>.

1450 Liu, Q., Reichle, R.H., Bindlish, R., Cosh, M.H., Crow, W.T., de Jeu, R., De Lannoy, G.J.M.,
1451 Huffman, G.J., Jackson, T.J., 2011. The contributions of precipitation and soil moisture
1452 observations to the skill of soil moisture estimates in a land data assimilation system. *J.*
1453 *Hydrometeorol.* 12, 750–765. <https://doi.org/10.1175/JHM-D-10-05000.1>.

1454 Lodh, A., Routray, A., Dutta, D., George, J.P., Mitra, A.K., 2022. Improving the prediction of
1455 monsoon depressions by assimilating ASCAT soil moisture in NCUM-R modeling
1456 system. *Atmos. Res.* 272, 106130. <https://doi.org/10.1016/j.atmosres.2022.106130>.

1457 Long, D., Bai, L., Yan, L., Zhang, C., Yang, W., Lei, H., Quan, J., Meng, X., Shi, C., 2019.
1458 Generation of spatially complete and daily continuous surface soil moisture of high
1459 spatial resolution. *Remote Sens. Environ.* 233, 111364.
1460 <https://doi.org/10.1016/j.rse.2019.111364>.

1461 Lorenc, A.C., Bowler, N.E., Clayton, A.M., Pring, S.R., Fairbairn, D., 2015. Comparison of
1462 hybrid-4DVar and hybrid-4DVar data assimilation methods for global NWP. *Mon.*
1463 *Weather Rev.* 143, 212–229. <https://doi.org/10.1175/MWR-D-14-00195.1>.

1464 Miller, D.A., White, R.A., 1998. A conterminous United States multilayer soil characteristics
1465 dataset for regional climate and hydrology modelling. *Earth Interact.* 2, 1–26.
1466 [https://doi.org/10.1175/1087-3562\(1998\)002<0001:ACUSMS>2.3.CO;2](https://doi.org/10.1175/1087-3562(1998)002<0001:ACUSMS>2.3.CO;2).

1467 Min, X., Shangguan, Y., Li, D., Shi, Z., 2022. Improving the fusion of global soil moisture
1468 datasets from SMAP, SMOS, ASCAT, and MERRA2 by considering the non-zero
1469 error covariance. *Int. J. Appl. Earth Obs.* 113, 103016.
1470 <https://doi.org/10.1016/j.jag.2022.103016>.

1471 Muñoz-Sabater, J., Lawrence, H., Albergel, C., de Rosnay, P., Isaksen, L., Mecklenburg, S. et
1472 al., 2019. Assimilation of SMOS brightness temperatures in the ECMWF integrated
1473 forecasting system. *Q. J. Roy. Meteor. Soc.* 145, 2524–2548.
1474 <https://doi.org/10.1002/QJ.3577>.

1475 Nair, A.S., Indu, J., 2018. A coupled land surface and radiative transfer models based on
1476 relief correction for a reliable land data assimilation over mountainous terrain. *IEEE*
1477 *Geosci. Remote Sens. Lett.* 15, 1657–1661.
1478 <https://doi.org/10.1109/LGRS.2018.2854908>.

- 1479 Nair, A.S., Indu, J., 2019. Improvement of land surface model simulations over India via data
 1480 assimilation of satellite-based soil moisture products. *J. Hydrol.* 573, 406–421.
 1481 <https://doi.org/10.1016/j.jhydrol.2019.03.088>.
- 1482 Nearing, G., Yatheendradas, S., Crow, W., Zhan, X., Liu, J., Chen, F., 2018. The efficiency
 1483 of data assimilation. *Water Resour. Res.* 54, 6374–6392.
 1484 <https://doi.org/10.1029/2017WR020991>.
- 1485 Nguyen, H.H., Kim, H., Crow, W., Yueh, S., Wagner, W., Lei, F., Wigneron, J.-P.,
 1486 Colliander, A., Frappart, F., 2025. From theory to hydrological practice: Leveraging
 1487 CYGNSS data over seven years for advanced soil moisture monitoring. *Remote Sens.*
 1488 *Environ.* 316, 114509. <https://doi.org/10.1016/j.rse.2024.114509>.
- 1489 O'Neill, P.E., Chan, S., Njoku, E.G., Jackson, T., Bindlish, R., Chaubell, J., 2021. SMAP L2
 1490 radiometer half-orbit 36 km EASE-grid soil moisture, version 8 [Data Set]. Boulder,
 1491 Colorado USA. NASA National Snow and Ice Data Center Distributed Active Archive
 1492 Center. <https://doi.org/10.5067/LPJ8F0TAK6E0>. Date Accessed 06-01-2023.
- 1493 Orth, R., Seneviratne, S.I., 2013. Propagation of soil moisture memory to streamflow and
 1494 evapotranspiration in Europe. *Hydrol. Earth Syst. Sci.* 17, 3895–3911.
 1495 <https://doi.org/10.5194/hess-17-3895-2013>.
- 1496 Pal, J.S., Eltahir, E.A.B., 2003. A feedback mechanism between soil-moisture distribution
 1497 and storm tracks. *Q. J. Roy. Meteor. Soc.* 129, 2279–2297.
 1498 <https://doi.org/10.1256/qj.01.201>.
- 1499 Paloscia, S., Pampaloni, P., 1988. Microwave polarization index for monitoring vegetation
 1500 growth. *IEEE Trans. Geosci. Remote Sens.* 26, 617–621.
 1501 <https://doi.org/10.1109/36.7687>.
- 1502 Peters-Lidard, C.D., Houser, P.R., Tian, Y., Kumar, S.V., Geiger, J., Olden, S., Lighty, L.,
 1503 Doty, B., Dirmeyer, P., Adams, J., Mitchell, K., Wood, E.F., Sheffield, J., 2007. High-
 1504 performance Earth system modeling with NASA/GSFC's land information system.
 1505 *Innov. Syst. Softw. Eng.* 3, 157–165. <https://doi.org/10.1007/s11334-007-0028-x>.
- 1506 Pipunic, R.C., Walker, J.P., Western, A.W., Trudinger, C.M., 2013. Assimilation of multiple
 1507 data types for improved heat flux prediction: a one-dimensional field study. *Remote*
 1508 *Sens. Environ.* 136, 315–329. <http://dx.doi.org/10.1016/j.rse.2013.05.015>.
- 1509 Polichtchouk, I., van Niekerk, A., Wedi, N., 2023. Resolved gravity waves in the
 1510 extratropical stratosphere: Effect of horizontal resolution increase from O(10) to O(1)
 1511 km. *J. Atmos. Sci.* 80, 473–486. <https://doi.org/10.1175/JAS-D-22-0138.1>.
- 1512 Reichle, R.H., McLaughlin, D.B., Entekhabi, D., 2002a. Hydrologic data assimilation with
 1513 the ensemble Kalman filter. *Mon. Weather Rev.* 130, 103–114.
 1514 [https://doi.org/10.1175/1520-0493\(2002\)130<0103:HDAWTE>2.0.CO;2](https://doi.org/10.1175/1520-0493(2002)130<0103:HDAWTE>2.0.CO;2).
- 1515 Reichle, R.H., Walker, J.P., Koster, R.D., Houser, P.R., 2002b. Extended versus ensemble
 1516 Kalman filtering for land data assimilation. *J. Hydrometeorol.* 3, 728–740.
 1517 [https://doi.org/10.1175/1525-7541\(2002\)003<0728:EVEKFF>2.0.CO;2](https://doi.org/10.1175/1525-7541(2002)003<0728:EVEKFF>2.0.CO;2).
- 1518 Reichle, R.H., Koster, R.D., 2004. Bias reduction in short records of satellite soil moisture.
 1519 *Geophys. Res. Lett.* 31, L19501. <https://doi.org/10.1029/2004GL020938>.
- 1520 Reichle, R.H., Koster, R.D., Liu, P., Mahanama, S.P.P., Njoku, E.G., Owe, M., 2007.
 1521 Comparison and assimilation of global soil moisture retrievals from the advanced

1522 microwave scanning radiometer for the earth observing system (AMSR-E) and the
1523 scanning multichannel microwave radiometer (SMMR). *J. Geophys. Res. Atmos.* 112,
1524 D09108. <https://doi.org/10.1029/2006JD008033>.

1525 Reichle, R.H., Crow, W.T., Koster, R.D., Sharif, H.O., Mahanama, S.P.P., 2008.
1526 Contribution of soil moisture retrievals to land data assimilation products. *Geophys.*
1527 *Res. Lett.* 35, L01404. <https://doi.org/10.1029/2007GL031986>.

1528 Reichle, R.H., Zhang, S.Q., Kolassa, J., Liu, Q., Todling, R., 2023. A weakly-coupled land
1529 surface analysis with SMAP radiance assimilation improves GEOS medium-range
1530 forecasts of near-surface air temperature and humidity. *Q. J. Roy. Meteor. Soc.* 149,
1531 1867–1889. <https://doi.org/10.1002/qj.4486>.

1532 Renzullo, L.J., van Dijk, A.I.J.M., Perraud, J.-M., Collins, D., Henderson, B., Jin, H., Smith,
1533 A.B., McJannet, D.L., 2014. Continental satellite soil moisture data assimilation
1534 improves root-zone moisture analysis for water resources assessment. *J. Hydrol.* 519,
1535 2747–2762. <https://doi.org/10.1016/j.jhydrol.2014.08.008>.

1536 Reynolds, C.A., Jackson, T.J., Rawls, W.J., 2000. Estimating soil water-holding capacities by
1537 linking the Food and Agriculture Organization Soil map of the world with global pedon
1538 databases and continuous pedotransfer functions. *Water Resour. Res.* 36, 3653–3662.
1539 <https://doi.org/10.1029/2000WR900130>.

1540 Rodell, M., Houser, P.R., Jambor, U., Gottschalck, J., Mitchell, K., Meng, C.-J., Arsenault,
1541 K., Cosgrove, B., Radakovich, J., Bosilovich, M., Entin, J.K., Walker, J.P., Lohmann,
1542 D., Toll, D., 2004. The Global Land Data Assimilation System. *Bull. Am. Meteorol.*
1543 *Soc.* 85, 381–394. <https://doi.org/10.1175/BAMS-85-3-381>.

1544 Santanello Jr., J.A., Kumar, S.V., Peters-Lidard, C.D., Lawston, P.M., 2016. Impact of soil
1545 moisture assimilation on land surface model spinup and coupled land–atmosphere
1546 prediction. *J. Hydrometeorol.* 17, 517–540. <https://doi.org/10.1175/JHM-D-15-0072.1>.

1547 Schmugge, T.J., O’Neill, P.E., Wang, J.R., 1986. Passive microwave soil moisture research.
1548 *IEEE Trans. Geosci. Remote Sens.* GE-24, 1.
1549 <http://dx.doi.org/10.1109/TGRS.1986.289584>.

1550 Scipal, K., Holmes, T., De Jeu, R., Naeimi, V., Wagner, W., 2008. A possible solution for the
1551 problem of estimating the error structure of global soil moisture data sets. *Geophys.*
1552 *Res. Lett.* 35, L24403, <https://doi.org/10.1029/2008GL035599>.

1553 Seo, E., Lee, M.-I., Reichle, R.H., 2021. Assimilation of SMAP and ASCAT soil moisture
1554 retrievals into the JULES land surface model using the Local Ensemble Transform
1555 Kalman Filter. *Remote Sens. Environ.* 253, 112222.
1556 <https://doi.org/10.1016/j.rse.2020.112222>.

1557 Shellito, P.J., Small, E.E., Cosh, M.H., 2016. Calibration of Noah soil hydraulic property
1558 parameters using surface soil moisture from SMOS and Basinwide in situ observations.
1559 *J. Hydrometeorol.* 17, 2275–2292. <https://doi.org/10.1175/JHM-D-15-0153.1>.

1560 Shellito, P.J., Small, E.E., Livneh, B., 2018. Controls on surface soil drying rates observed by
1561 SMAP and simulated by the Noah land surface model. *Hydrol. Earth Syst. Sci.* 22,
1562 1649–1663. <https://doi.org/10.5194/hess-22-1649-2018>.

- 1563 Shin, Y., Jung, Y., 2014. Development of irrigation water management model for reducing
1564 drought severity using remotely sensed soil moisture footprints *J. Irrig. Drain. Eng.* 140,
1565 04014021. [https://doi.org/10.1061/\(ASCE\)IR.1943-4774.0000736](https://doi.org/10.1061/(ASCE)IR.1943-4774.0000736).
- 1566 Singh, A., Gaurav, K., 2023. Deep learning and data fusion to estimate surface soil moisture
1567 from multi-sensor satellite images. *Sci. Rep.* 13, 2251. <https://doi.org/10.1038/s41598-023-28939-9>.
- 1569 Song, H.-J., Shin, S., Ha, J.-H., Lim, S., 2017. The advantages of hybrid 4DEnVar in the
1570 context of the forecast sensitivity to initial conditions. *J. Geophys. Res. Atmos.* 122,
1571 12226–12244. <https://doi.org/10.1002/2017JD027598>.
- 1572 Stoffelen, A., 1998. Toward the true near-surface wind speed: error modeling and calibration
1573 using triple collocation. *J. Geophys. Res.* 103, 7755–7766.
1574 <https://doi.org/10.1029/97JC03180>.
- 1575 Tangdamrongsub, N., Han, S.-C., Yeo, I.-Y., Dong, J., Steele-Dunne, S.C., Willgoose, G.,
1576 Walker, J.P., 2020. Multivariate data assimilation of GRACE, SMOS, SMAP
1577 measurements for improved regional soil moisture and groundwater storage estimates.
1578 *Adv. Water Resour.* 135, 103477. <https://doi.org/10.1016/j.advwatres.2019.103477>.
- 1579 Tuttle, S., Salvucci, G., 2016. Empirical evidence of contrasting soil moisture–precipitation
1580 feedbacks across the United States. *Science* 352, 825–828.
1581 <https://doi.org/10.1126/science.aaa7185>.
- 1582 van den Hurk, B., Doblas-Reyes, F., Balsamo, G., Koster, R.D., Seneviratne, S.I., Camargo Jr,
1583 H., 2012. Soil moisture effects on seasonal temperature and precipitation forecast
1584 scores in Europe. *Climate Dyn.* 38, 349–362. <https://doi.org/10.1007/s00382-010-0956-2>.
- 1586 van der Schalie, R., de Jeu, R., Rodríguez-Fernández, N., Al-Yaari, A., Kerr, Y., Wigneron,
1587 J.-P., Parinussa, R., Drusch, M., 2018. The Effect of three different data fusion
1588 approaches on the quality of soil moisture retrievals from multiple passive microwave
1589 sensors. *Remote Sens.* 10, 107. <https://doi.org/10.3390/rs10010107>.
- 1590 Wagner, W., Lemoine, G., Rott, H., 1999. A method for estimating soil moisture from ERS
1591 scatterometer and soil data. *Remote Sens. Environ.* 70, 191–207.
1592 [https://doi.org/10.1016/S0034-4257\(99\)00036-X](https://doi.org/10.1016/S0034-4257(99)00036-X).
- 1593 Wagner, W., Bartalis, Z., Naeimi, V., Park, S.-E., Figa-Saldaña, J., Bonekamp, H., 2010.
1594 Status of the MetOp ASCAT soil moisture product. *IEEE Int. Geosci. Remote. Se.*
1595 *Proceedings.* 25-30 July 2010, 276–279.
1596 <https://doi.org/10.1109/IGARSS.2010.5653358>.
- 1597 Wagner, W., Hahn, S., Kidd, R., Melzer, T., Bartalis, Z., Hasenauer, S., Figa-Saldaña, J., De
1598 Rosnay, P., Jann, A., Schneider, S., Komma, J., Kubu, G., Brugger, K., Aubrecht, C.,
1599 Züger, J., Gangkofner, U., Kienberger, S., Brocca, L., Wang, Y., Blöschl, G., Eitzinger,
1600 J., Steinnocher, K., Zeil, P., Rubel, F., 2013. The ASCAT soil moisture product: A
1601 review of its specifications, validation results, and emerging applications.
1602 *Meteorologische Zeitschrift* 22, 5–33. <https://doi.org/10.1127/0941-2948/2013/0399>.
- 1603 Wagner, W., Lindorfer, R., Hahn, S., Kim, H., Vreugdenhil, M., Gruber, A., Fischer, M.,
1604 Trnka, M., 2024. Global scale mapping of subsurface scattering signals impacting

1605 ASCAT soil moisture retrievals. *IEEE Trans. Geosci. Remote Sens.* 62, 4509520.
1606 <https://doi.org/10.1109/TGRS.2024.3429550>.

1607 Wanders, N., Karssenber, D., de Roo, A., de Jong, S.M., Bierkens, M.F.P., 2014. The
1608 suitability of remotely sensed soil moisture for improving operational flood forecasting,
1609 *Hydrol. Earth Syst. Sci.* 18, 2343–2357. <https://doi.org/10.5194/hess-18-2343-2014>.

1610 Wang, Y., Mao, J., Jin, M., Hoffman, F.M., Shi, X., Wulschleger, S.D., Dai, Y., 2021.
1611 Development of observation-based global multilayer soil moisture products for 1970 to
1612 2016. *Earth Syst. Sci. Data* 13, 4385–4405. <https://doi.org/10.5194/essd-13-4385-2021>.

1613 WMO, 2008. Recommendations for the verification and intercomparison of QPFs and PPFs
1614 from operational NWP models. WWRP 2009-1, World Meteorological Organization
1615 (WMO), Switzerland.

1616 Wu, K., Ryu, D., Nie, L., Shu, H., 2021. Time-variant error characterization of SMAP and
1617 ASCAT soil moisture using Triple Collocation Analysis. *Remote Sens. Environ.* 256,
1618 112324. <https://doi.org/10.1016/j.rse.2021.112324>.

1619 Xie, P., Yatagai, A., Chen, M., Hayasaka, T., Fukushima, Y., Liu, C., Yang, S., 2007. A
1620 gauge-based analysis of daily precipitation over East Asia. *J. Hydrometeorol.* 8, 607–
1621 626. <https://doi.org/10.1175/JHM583.1>.

1622 Xie, Q., Jia, L., Menenti, M., Hu, G., 2022. Global soil moisture data fusion by Triple
1623 Collocation Analysis from 2011 to 2018. *Sci. Data* 9, 687.
1624 <https://doi.org/10.1038/s41597-022-01772-x>.

1625 Xu, T., Chen, F., He, X., Barlage, M., Zhang, Z., Liu, S., He, X., 2021. Improve the
1626 performance of the Noah-MP-Crop model by jointly assimilating soil moisture and
1627 vegetation phenology data. *J. Adv. Model. Earth Sy.* 13, e2020MS002394.
1628 <https://doi.org/10.1029/2020MS002394>.

1629 Yang, L., Sun, G., Zhi, L., Zhao, J., 2018. Negative soil moisture-precipitation feedback in
1630 dry and wet regions. *Sci. Rep.* 8, 4026. <https://doi.org/10.1038/s41598-018-22394-7>.

1631 Yin, J., Hain, C.R., Zhan, X., Dong, J., Ek, M., 2019. Improvements in the forecasts of near-
1632 surface variables in the Global Forecast System (GFS) via assimilating ASCAT soil
1633 moisture retrievals. *J. Hydrol.* 578, 124018.
1634 <https://doi.org/10.1016/j.jhydrol.2019.124018>.

1635 Yuan, X., Wood, E.F., Luo, L., Pan, M., 2011. A first look at Climate Forecast System
1636 version 2 (CFSv2) for hydrological seasonal prediction. *Geophys. Res. Lett.* 38,
1637 L13402. <https://doi.org/10.1029/2011GL047792>.

1638 Zhang, H., Wang, S., Liu, K., Li, X., Li, Z., Zhang, X., Liu, B., 2022. Downscaling of
1639 AMSR-E soil moisture over north China using random forest regression. *ISPRS Int. J.*
1640 *Geo Inf.* 11, 101. <https://doi.org/10.3390/ijgi11020101>.

1641 Zheng, J., Yuan, X., Ji, P., 2024. The important role of reliable land surface model simulation
1642 in high-resolution multi-source soil moisture data fusion by machine learning. *J.*
1643 *Hydrol.* 630, 130700. <https://doi.org/10.1016/j.jhydrol.2024.130700>.